The Thermohaline Circulation and Rapid Climate Change

Thermohaline Circulation

Stommel Model

Multiple Steady States in GCM

The Recent Climate History: Rapid Changes

Possible explanations

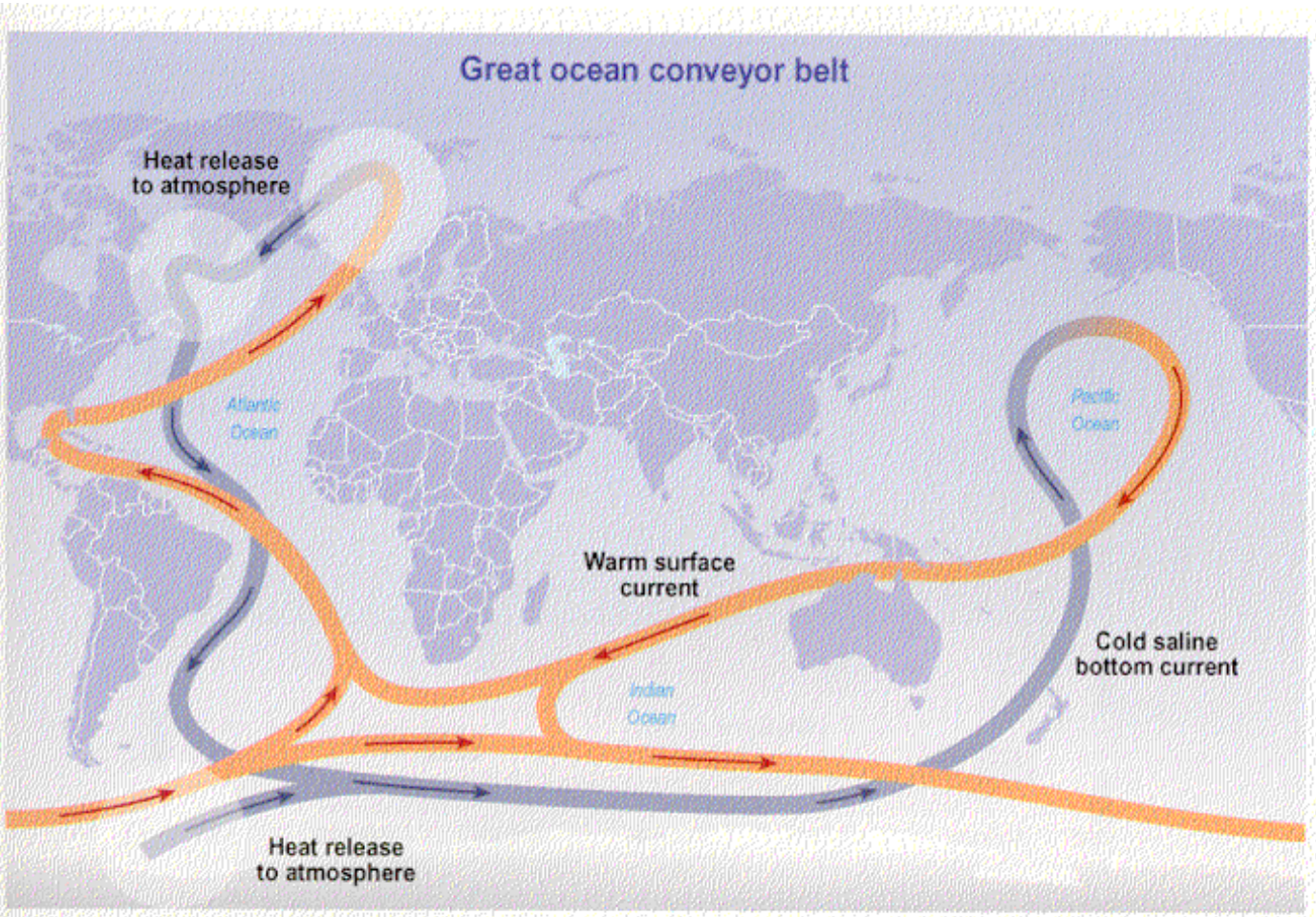

PLATE 4a The great ocean conveyor belt. This is a schematic generally summarizing some important features of the world's ocean circulation. Warm, low-salinity water, flows north along the surface of the Atlantic, becoming saltier (red arrows). Cooling of this to saltier water in the North Atlantic produces high enough densities for the water to sink and flow southward in the deep ocean and into other ocean basins (blue arrows) (after Broecker, 1995).

North Atlanic salinity is hight and N. Pacific salinity low due to fresh water flux and THC

Alley et al., Abrupt Climate Change, NAP, 2002

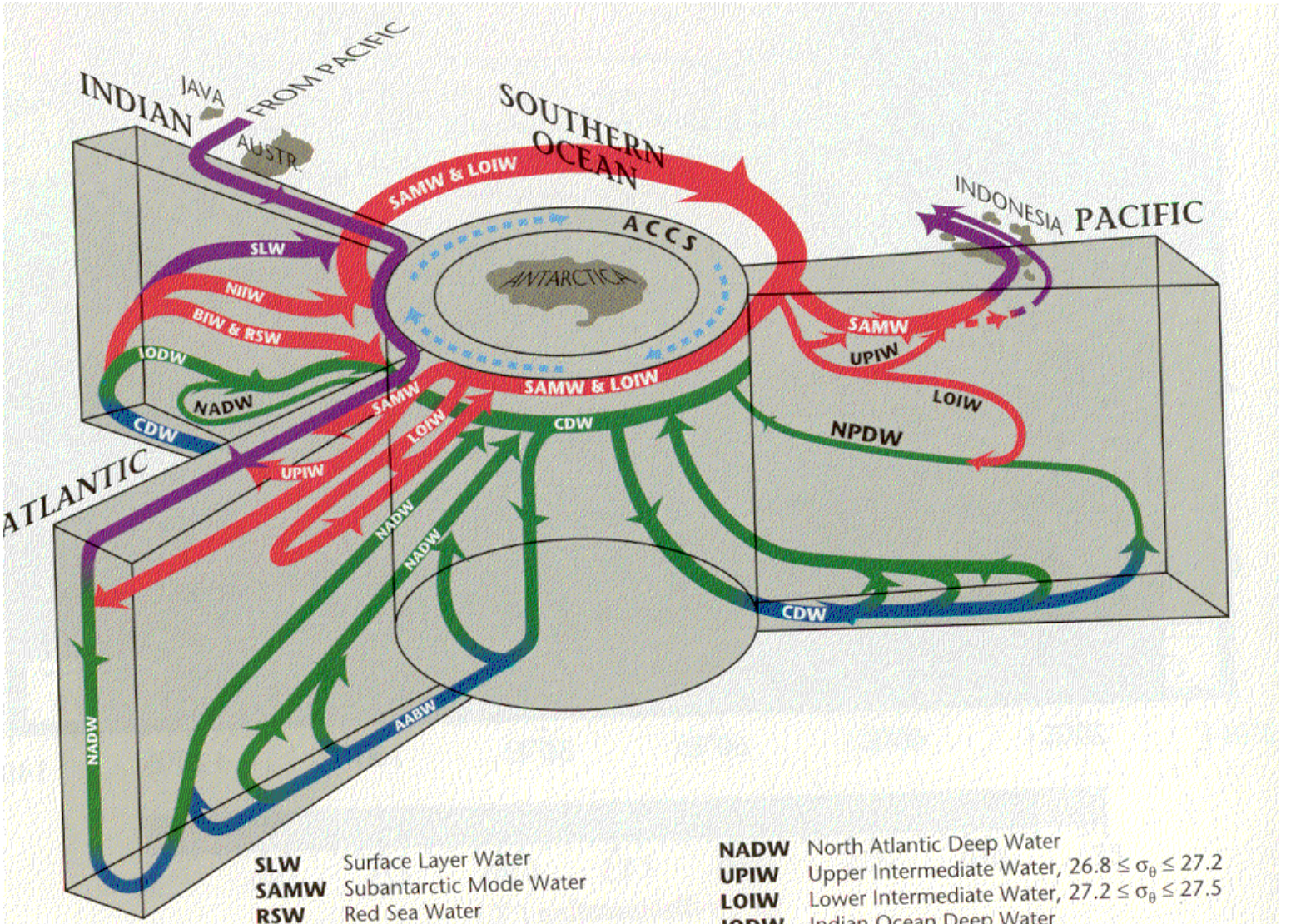

SLW	Surface Layer Water	**NADW**	North Atlantic Deep Water
SAMW	Subantarctic Mode Water	**UPIW**	Upper Intermediate Water, $26.8 \le \sigma_\theta \le 27.2$
RSW	Red Sea Water	**LOIW**	Lower Intermediate Water, $27.2 \le \sigma_\theta \le 27.5$
AABW	Antarctic Bottom Water	**IODW**	Indian Ocean Deep Water
NPDW	North Pacific Deep Water	**BIW**	Banda Intermediate Water
ACCS	Antarctic Circumpolar Current System	**NIIW**	Northwest Indian Intermediate Water
CDW	Circumpolar Deep Water		

Figure II-8: A three-dimensional interbasin flow schematic with "typical" meridional–vertical sections for the indicated oceans, and their horizontal connections in the Southern Ocean and the Indonesian Passages. The surface layer circulations are in purple, intermediate and SAMW are in red, deep in green, and near bottom in blue.

Schmitz, WHOI Tech Rep. 96-08, 1996

Surface boundary conditions for temperature and salinity

Temperature (Haney 1971)

$$Q = Q(T) = Q_I + \frac{\partial Q}{\partial T}|_{T=T_a}(T_a - T)$$

$$Q = \frac{\partial Q}{\partial T}(T^* - T)$$

$$T^* = T_a + Q_I \, (\frac{\partial Q}{\partial T})^{-1}$$

In the limiting case of very fast feedback, the upper ocean temperature is prescribed.

Salinity

$$E - P = (E - P)_0 + \frac{\partial (E - P)}{\partial S}|_{S_a}(S_a - T)$$

Since feedback term is so small, the fresh water flux is presribed independent of the state of the ocean's salinity.

Effects of mixed surface boundary conditions: Stommel (1961)

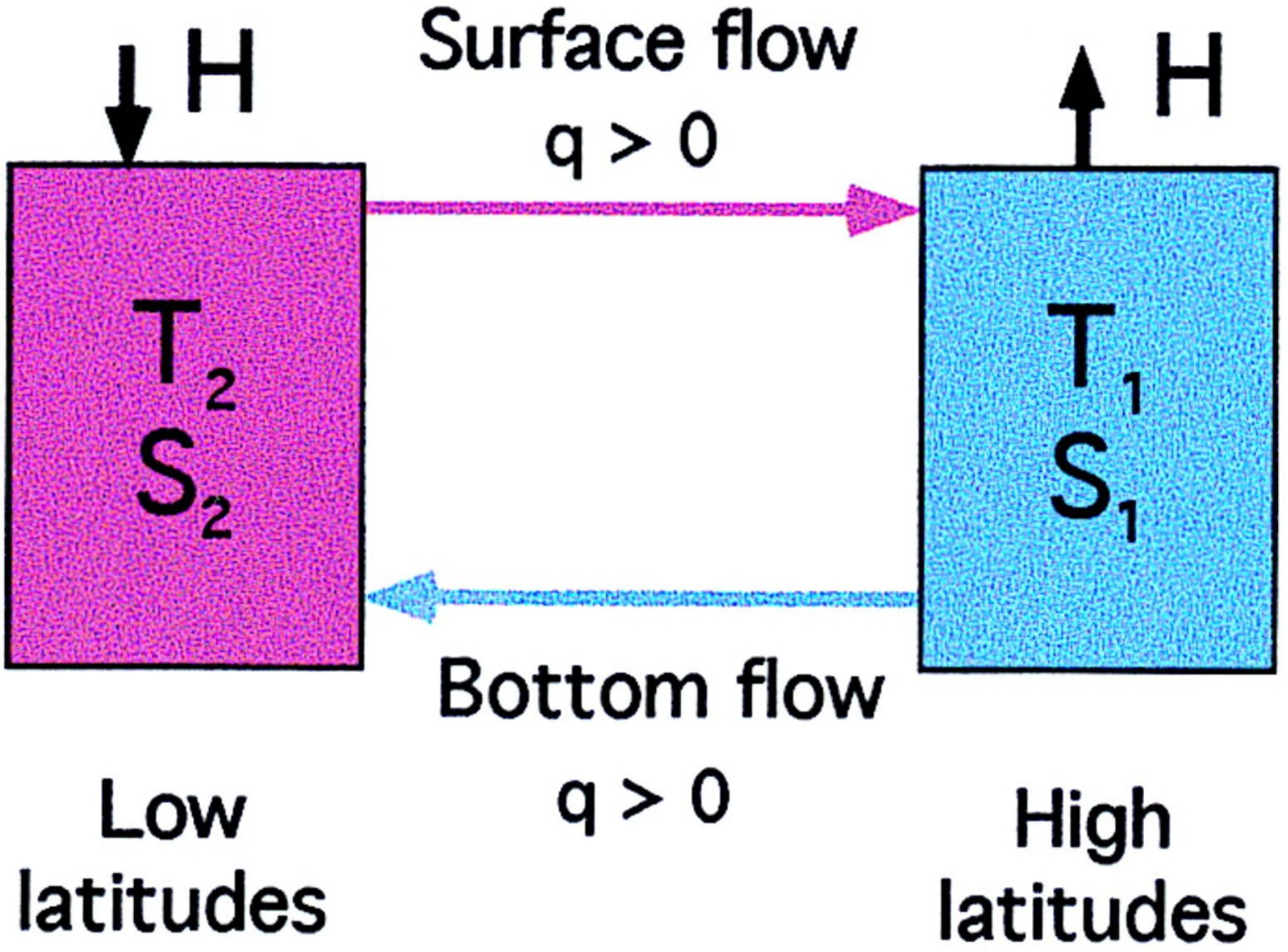

Which of the opposing temperature and salinity contrasts dominate the density difference and THC?

Marotzke, PNAS, 2000

Stommel (1961) model

For fast temperature feedback, such that temperatures are constant at T_1, T_2

$$V\frac{dS_1}{dt} = -FS_0 + |q|(S_2 - S_1)$$
$$V\frac{dS_2}{dt} = FS_0 - |q|(S_2 - S_1)$$
$$q = -\frac{k}{\rho_0}(\rho_2 - \rho_1)$$
$$\rho = \rho_0(1 - \alpha T + \beta S)$$

and parameters

$$\delta = \frac{\beta(S_2 - S_1)}{\alpha(T_2 - T_1)} \quad \textit{Salinity gradient}$$
$$r = \frac{q}{k\alpha(T_2 - T_1)} \quad \textit{Circulation}$$
$$E = \frac{\beta FS_0}{kV[\alpha(T_2 - T_1)]^2} \quad \textit{Fresh-water forcing}$$
$$2k\alpha(T_2 - T_1) \quad \textit{time-scale}$$

this system for the pole to equator salinity difference reduces to

$$\frac{d\delta}{dt} = E - |r|\delta$$
$$r = 1 - \delta$$

with three steady solution, two of which are stable

$$\delta_1 = \frac{1}{2}(1 - \sqrt{1 - 4E})$$
$$\delta_2 = \frac{1}{2}(1 + \sqrt{1 - 4E})$$
$$\delta_3 = \frac{1}{2}(1 + \sqrt{1 + 4E})$$

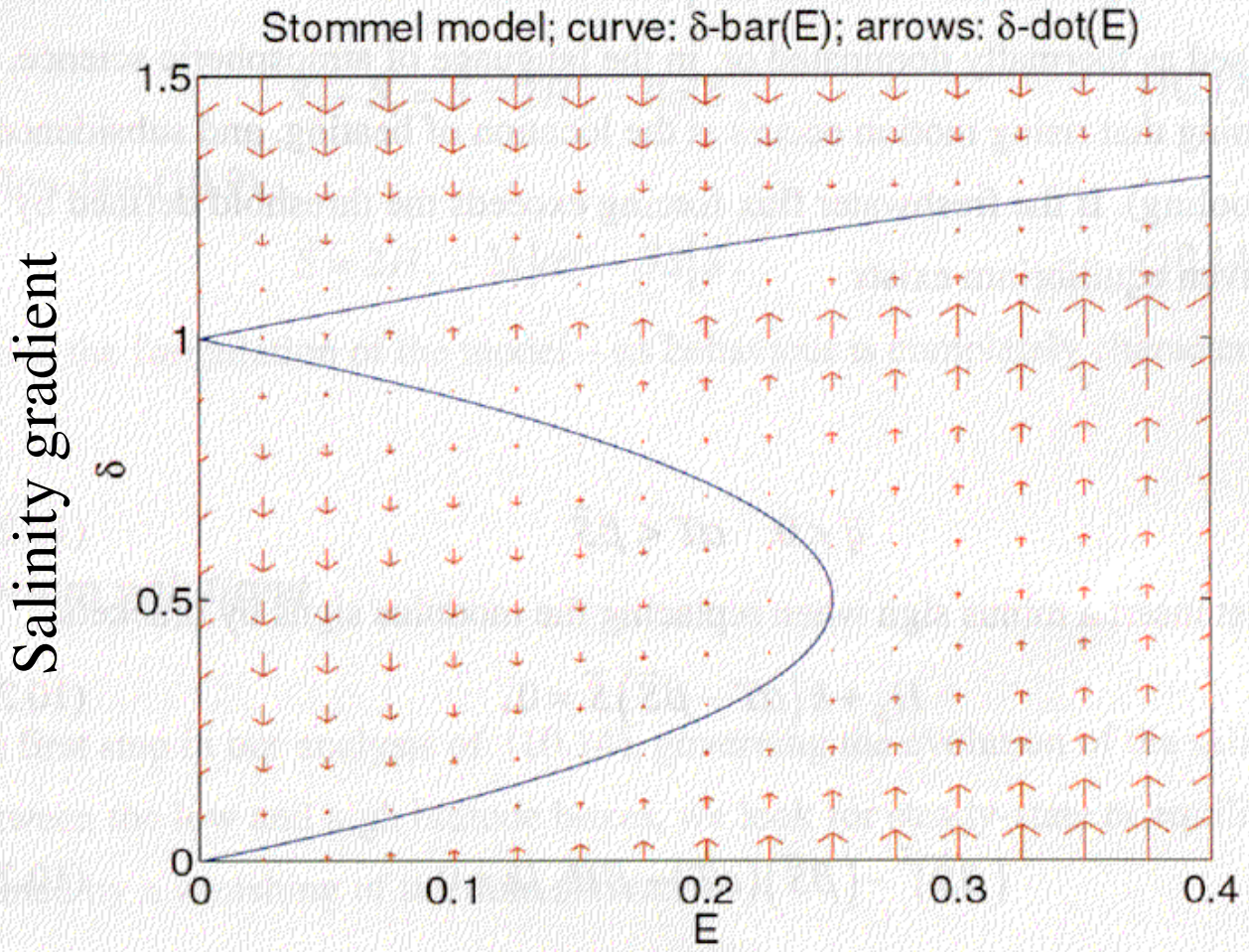

Figure 10.2 Solution portrait of the box model in phase space. Dimensionless salinity difference is denoted $\delta \equiv \beta S / \alpha T$; dimensionless surface salinity flux is $E \equiv \beta H_s / k(\alpha T)^2$. The curves mark the equilibrium solutions, $\overline{\delta}(E)$, while the arrows show the tendencies in phase space. Notice the existence of three steady states for E < ¼.

Marotzke, Lecture Notes, 2003

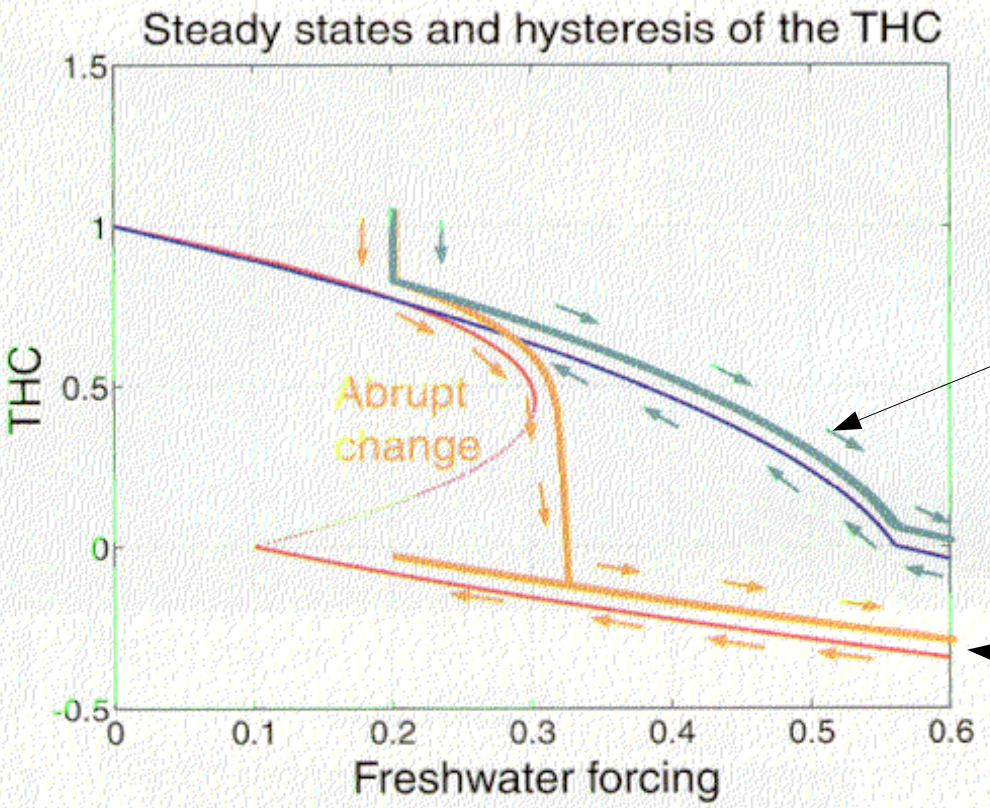

Strong diffusion

Weak diffusion

PLATE 6 Paths along the solution curves of two versions of Stommel's box model showing the rate of the ocean overturning when the freshwater forcing flux H is increased and then decreased. Only in the case of weak diffusion (orange) does the model respond with an abrupt change, once a threshold in H is crossed. In the case of strong diffusion (green), at any time, there is a unique equilibrium.

Alley et al., Abrupt Climate Change, NAP, 2002

Pole to pole density gradient (Rooth 1982)

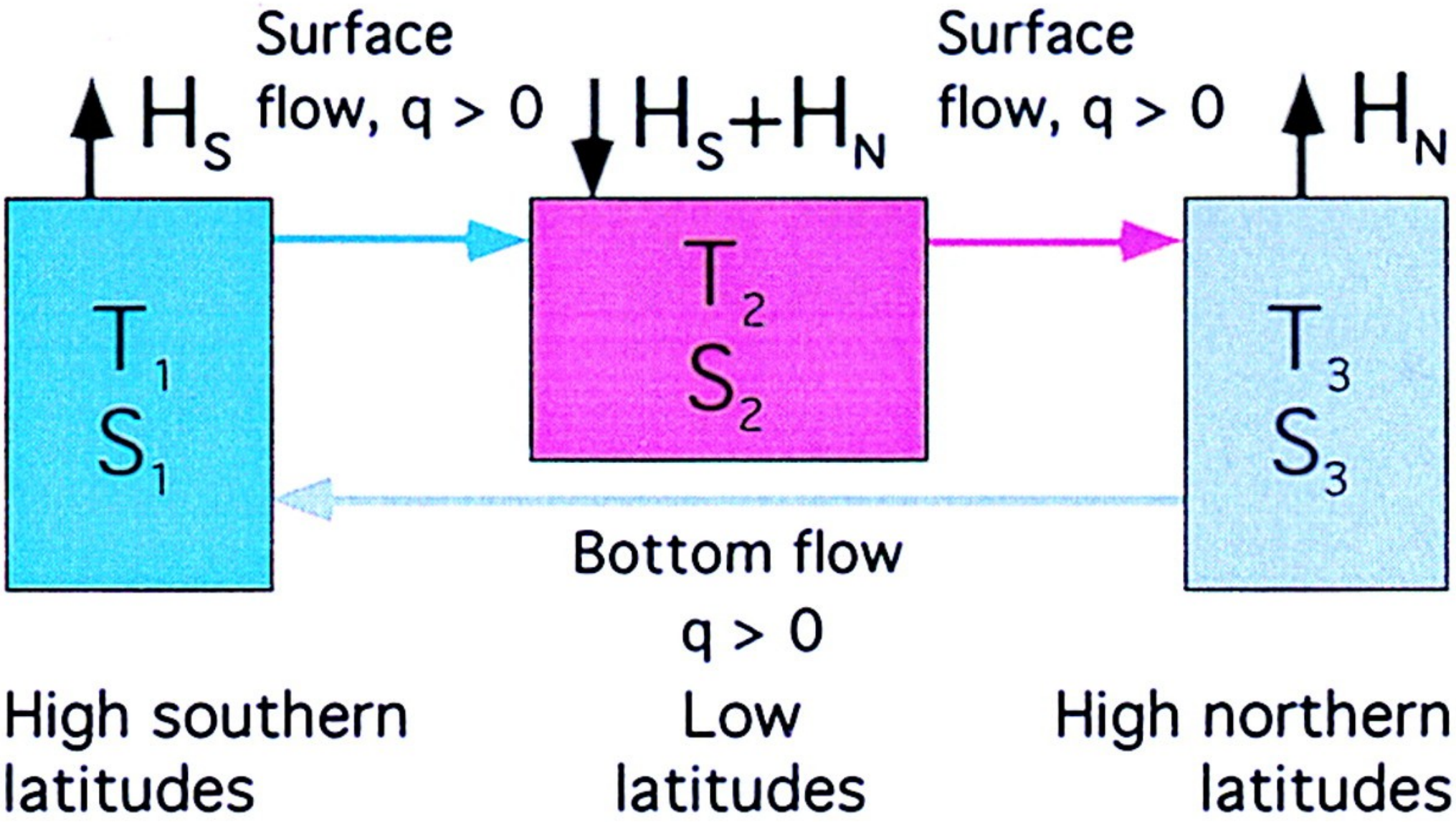

Marotzke, PNAS, 2000

Rooth's model: instability of symmetric state

Symmetry requires that q = 0, i.e. Salinity in each box increases linearly with time. Any perturbation, say in the northern box, leads to an increase of the flow advecting salty, 'low latitude', water into the northern box, which further increases the initial perturbation.

Asymmetric state

Steady response of the flow depends only on the 'southern' hemisphere moisture flux. The model can not sustain the sense of circulation if ratio of 'southern' to 'northern' salinity forcing is too large. If the 'northern' hemisphere receives too much fresh water, the sense of circulation has to be reversed.

Can the instability of the THC be reproduced in GCM simulations?

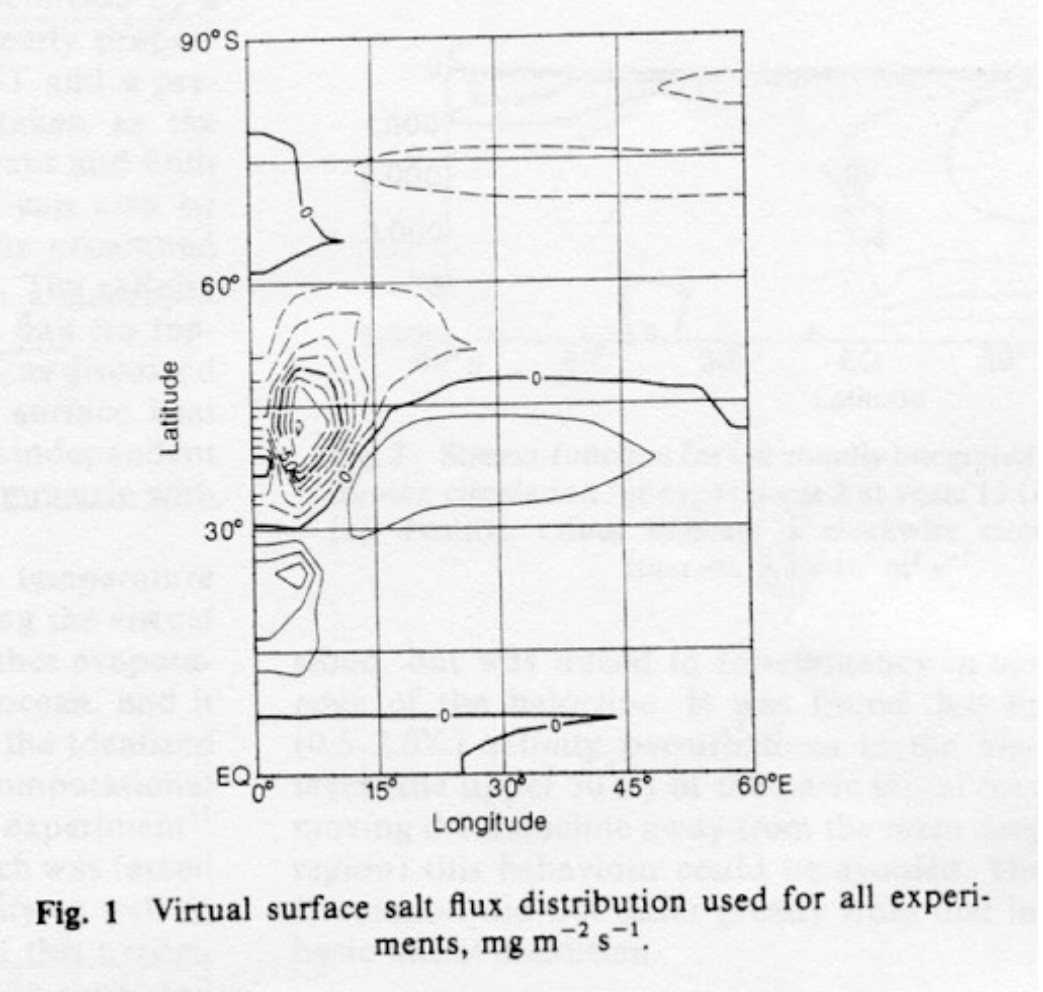

Fig. 1 Virtual surface salt flux distribution used for all experiments, mg m^{-2} s^{-1}.

Bryan, Nature, 1986

Exp. 1: initialize model with symmetric state and apply symmetric perturbation:
Model remains in symmetric state

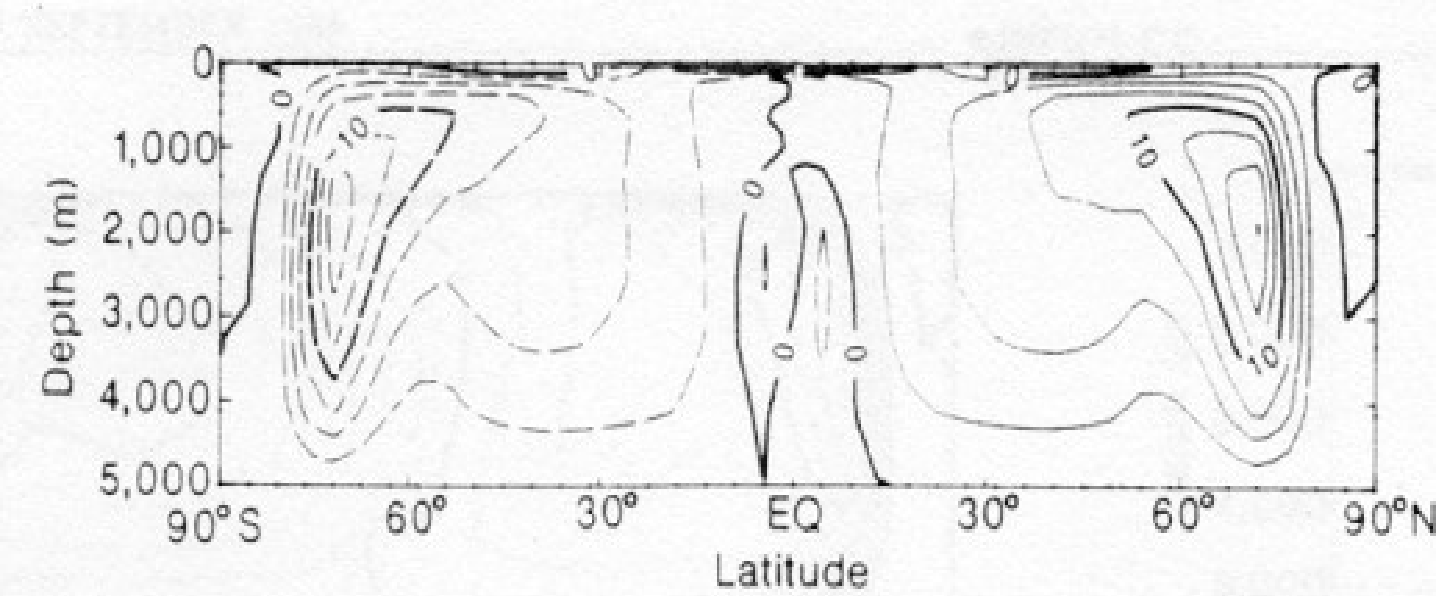

Fig. 2 Stream-function for the zonally integrated meridional overturning circulation for experiment 1 at the end of the integration. Positive values indicate a clockwise circulation; contour interval, $2.5 \times 10^6\ m^3\ s^{-1}$.

Bryan, Nature,

Add fresh anomaly

Convection in SH is suppressed, residence time at surface is increased, and THC collapses due to lack of convection. Fast positive feedback.

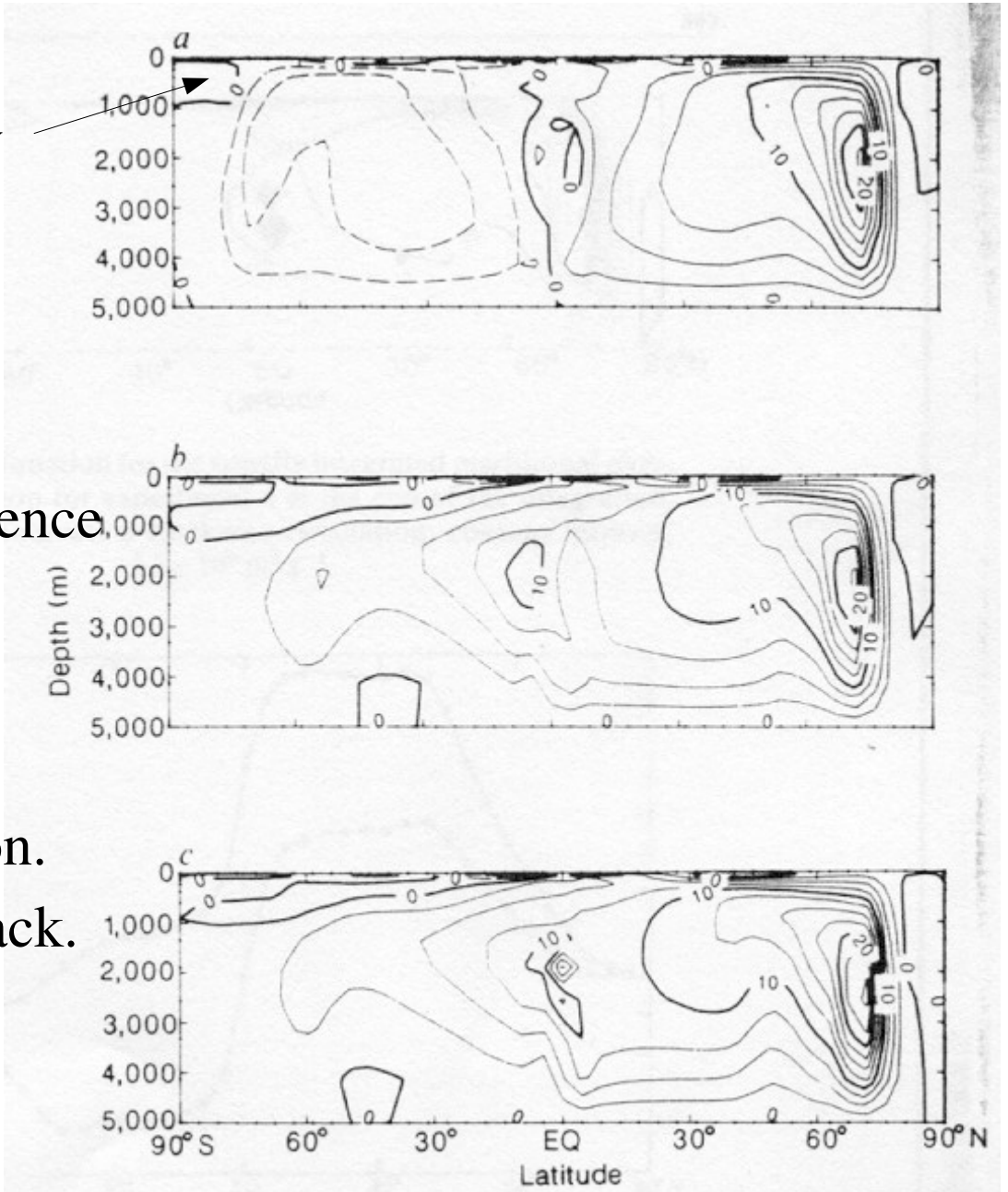

Fig. 3 Stream-function for the zonally integrated meridional overturning circulation for experiment 2 at years 15 (*a*), 44 (*b*) and 68 (*c*). Positive values indicate a clockwise circulation; contour interval, 2.5×10^6 m^3 s^{-1}.

Bryan, Nature, 1986

Add salty anomaly

Salty anomaly is mixed vertically, and increases THC slightly, again leading to a asymmetric state, but with a much slower growth rate.

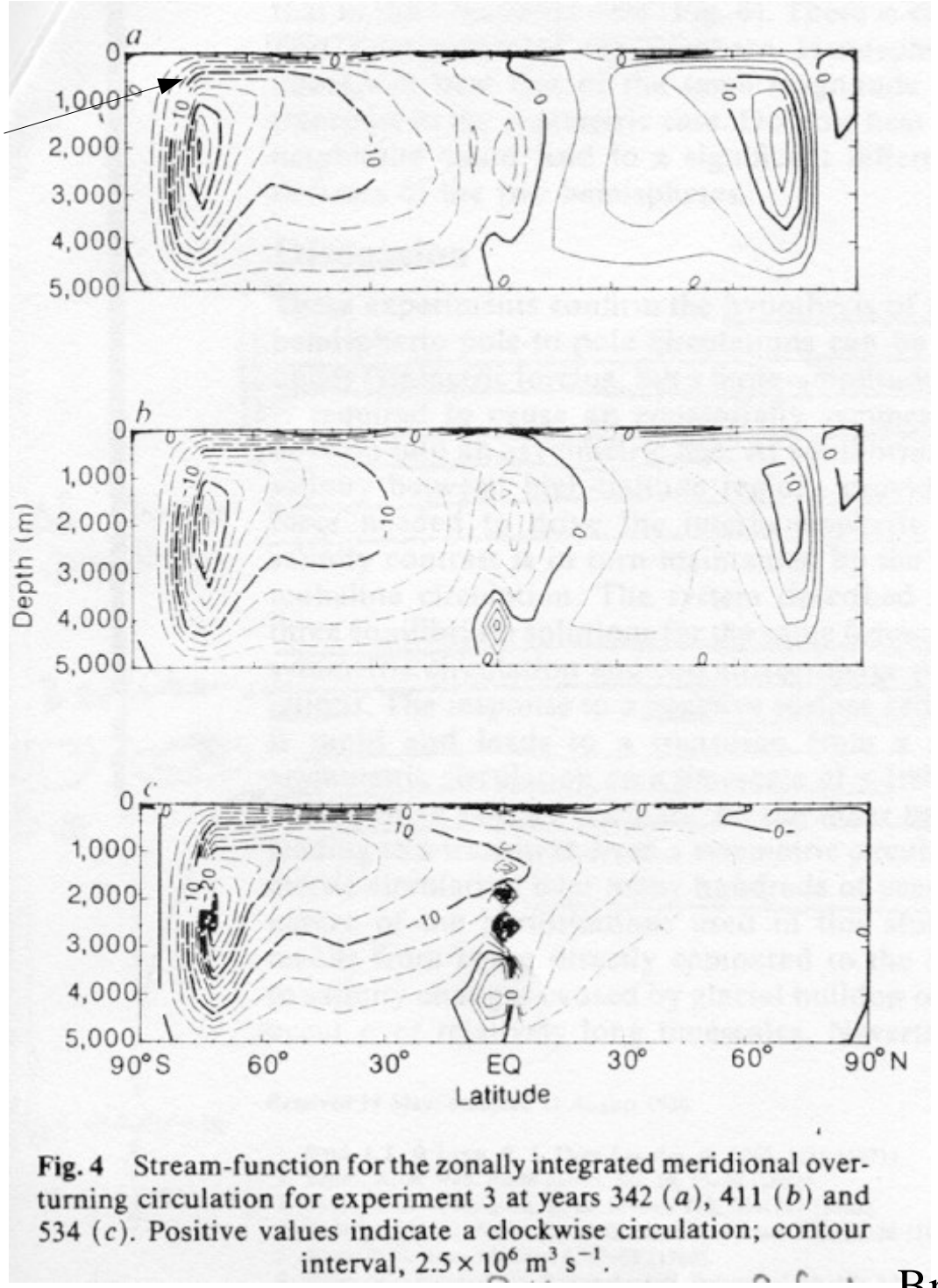

Fig. 4 Stream-function for the zonally integrated meridional overturning circulation for experiment 3 at years 342 (*a*), 411 (*b*) and 534 (*c*). Positive values indicate a clockwise circulation; contour interval, 2.5×10^6 m^3 s^{-1}.

Bryan, Nature, 1986

Add salt in north

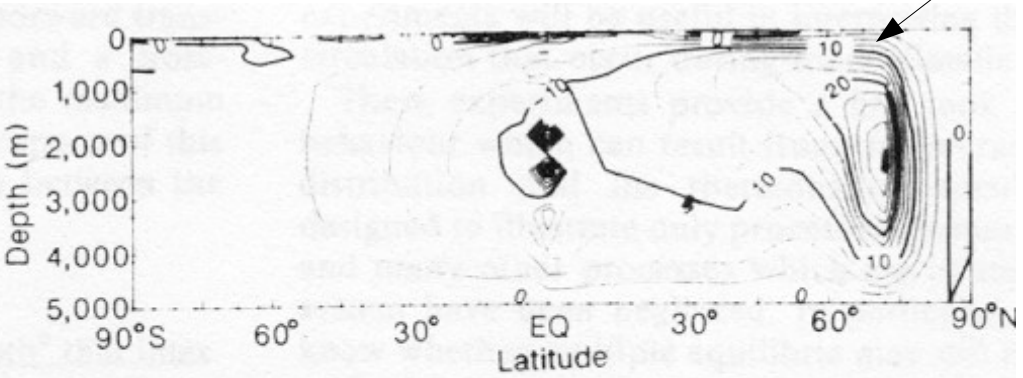

Fig. 5 Stream-function for the zonally integrated meridional overturning circulation for experiment 4 at the end of the integration. Positive values indicate a clockwise circulation; contour interval, 2.5×10^6 m^3 s^{-1}.

Bryan, Nature, 1986

Heat transport differs dramatically between symmetric and asymmetric THC.

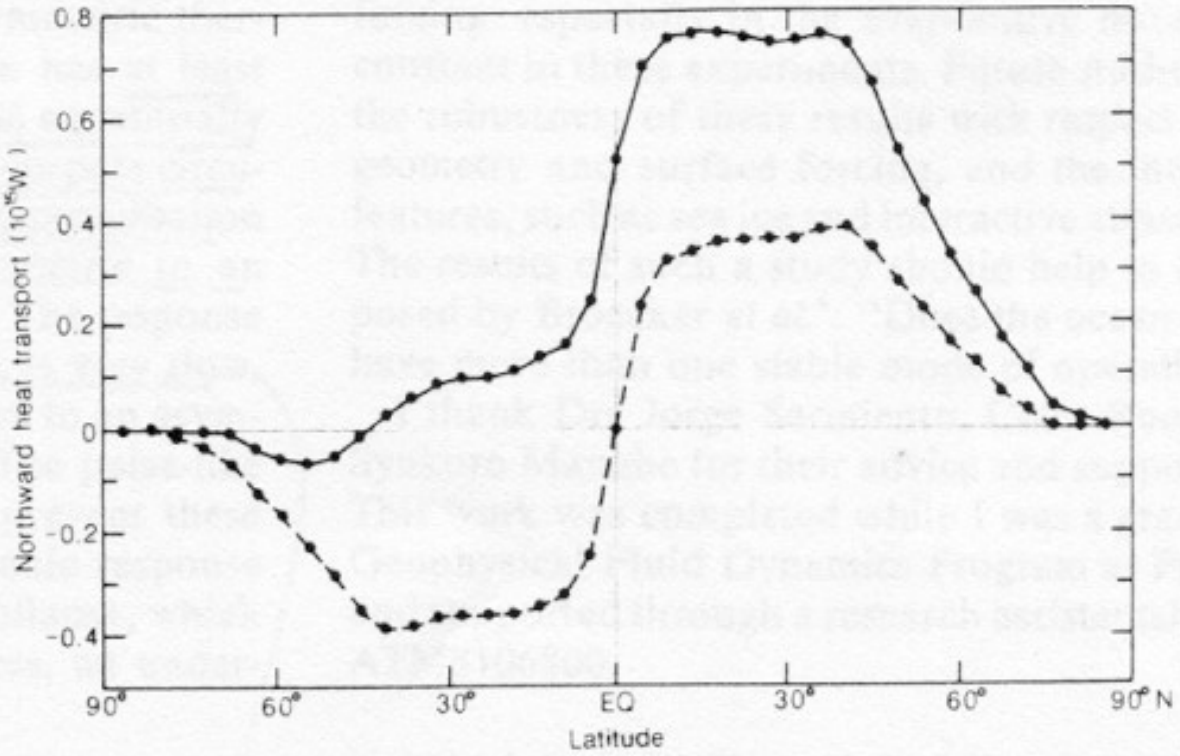

Fig. 6 Northward heat transport for experiment 4 (solid line) at the end of the integration, and for the symmetric solution obtained with newtonian-cooling-type boundary conditions on both temperature and salinity (dashed line).

Bryan, Nature, 1986

Response of coupled model to freshening in the North Atlantic

Increased fresh water flux of 1Sv for ten years

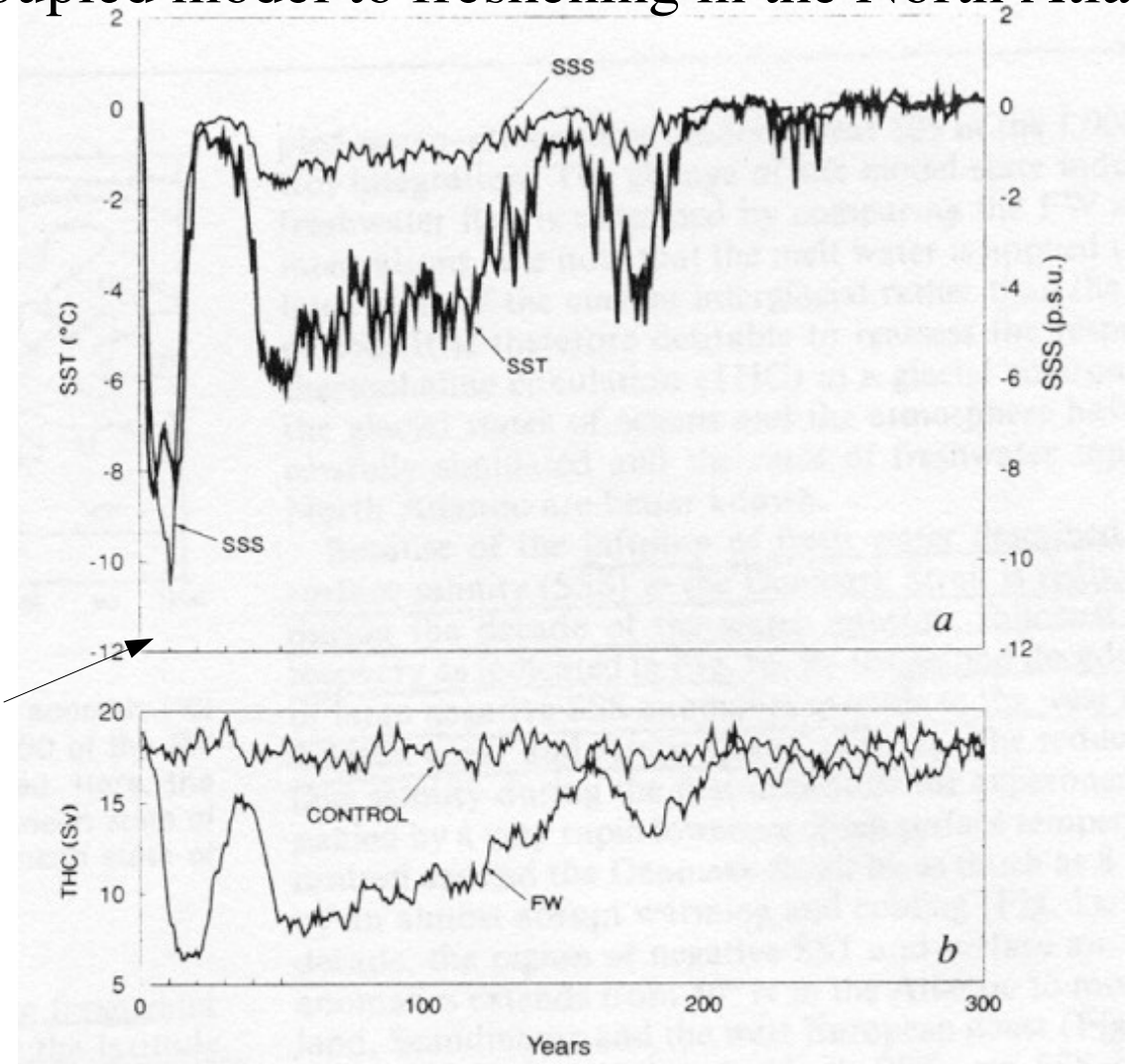

FIG. 1 *a*, Time series of the deviations of sea surface temperature (SST) and sea surface salinity (SSS; p.s.u., practical salinity units) from their initial values (that is, 7 °C and 35 p.s.u., respectively) at a grid point in the Denmark Strait (60.75° N, 37.50° W) obtained from the FW experiment. *b*, Temporal variations of the rate of THC in the North Atlantic obtained from the control and FW integrations. Here, the rate of THC is defined as the maximum value of the stream function of meridional circulation in the North Atlantic (Fig. 4).

Manabe and Stouffer, Nature, 1995

Surface salinity anomalies

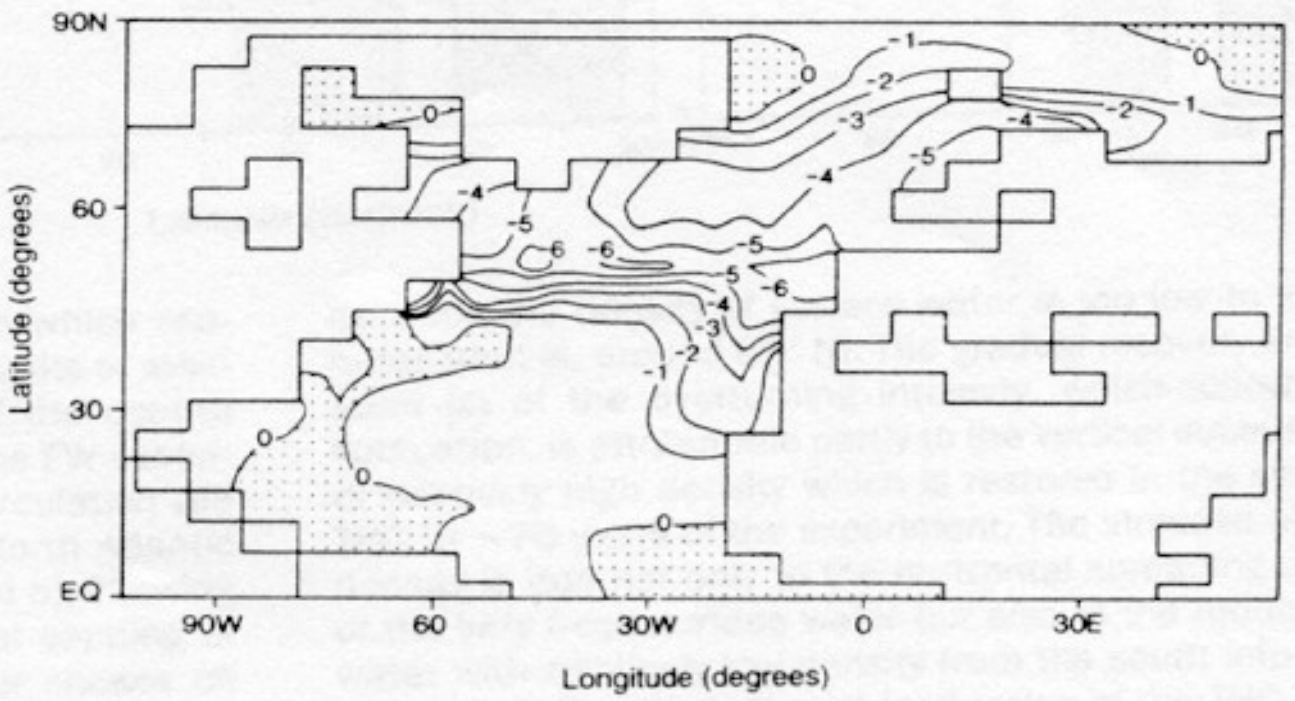

FIG. 2 Horizontal distribution of SSS anomalies (in units of p.s.u.) averaged over the 10-year period from year 11 to year 20 of the FW experiment. The areas of positive anomalies are shaded. Here, the anomaly represents the difference between the 10-year mean state of the FW integration and the 100-year (years 501–600) mean state of the control integration.

Manabe and Stouffer, Nature, 1995

Resulting anomalies of surface temperature

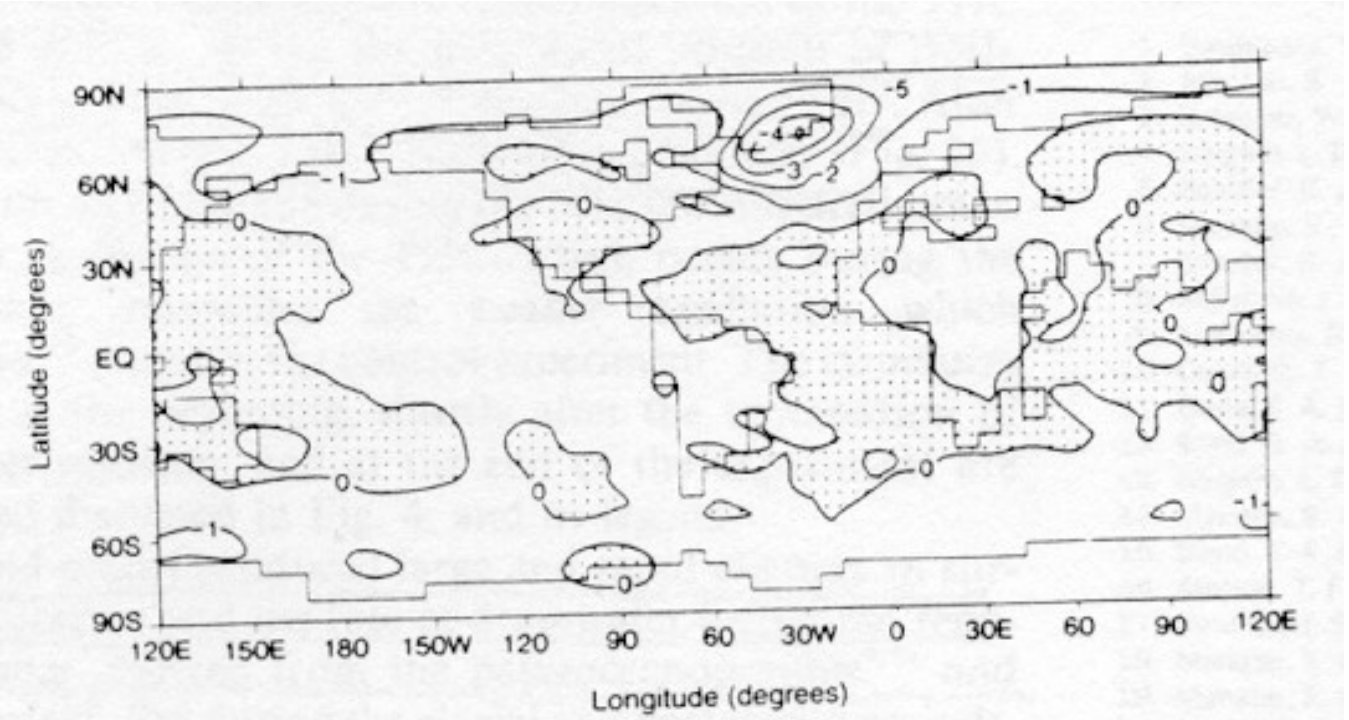

FIG. 3 Horizontal distribution of surface air temperature anomaly (°C) averaged over the 10-year period from year 51 to year 60 of the FW experiment. The areas of positive anomalies are shaded. Here, the anomaly represents the difference between the 10-year mean state of the FW integration and the 100-year (years 501–600) mean state of the control integration.

Manabe and Stouffer, Nature, 1995

Reduction of THC due to freshwater flux

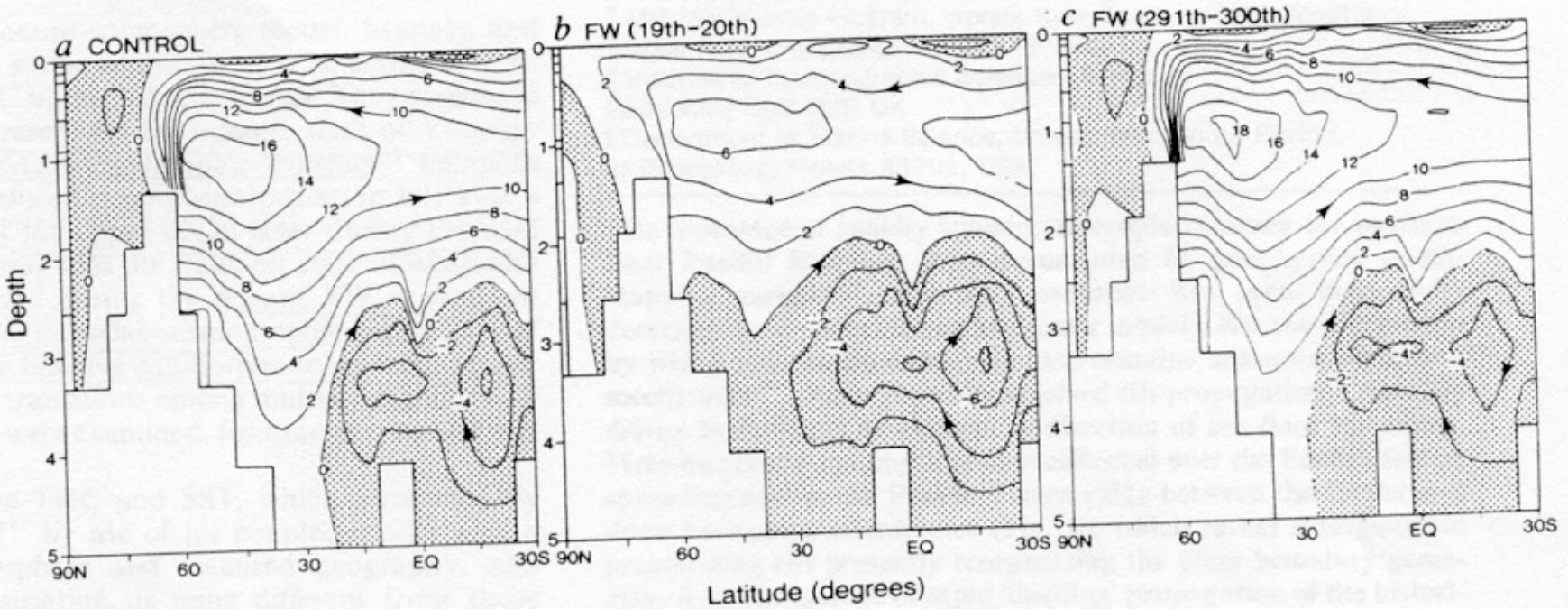

FIG. 4 Latitude–depth distribution of the stream function which represents the meridional overturning in the North Atlantic in units of sverdrups (10^6 m^3 s^{-1}), averaged over: *a*, years 501–600 of the control experiment; *b*, years 19 and 20 and *c*, years 291–300 of the FW experiment. (Depth is given in kilometres; areas of clockwise circulation are shaded.) During the few initial decades, the THC in the North Atlantic markedly weakens and becomes shallower (compare *a* and *b*), allowing stronger deep inflow of Antarctic bottom water. The initial capping of the Atlantic Ocean by the low-density, fresh surface water chokes off the heat exchange between the atmosphere and ocean and raises the temperature of subsurface water, rapidly weakening the THC during the first decade of the experiment. At the end of the second decade, the THC extends poleward of 65° N in the near-surface layer (*b*). The associated extension of the northward advection of warm surface water is responsible for the rapid increase of SST and SSS in the Greenland Sea during the second decade (Fig. 1*a*). The northward extension of warm advection disappears by year 40 of the experiment, causing the reduction of SST and SSS during the fourth decade (Fig. 1*a*). It appears that the northward extension (into the Norwegian/Greenland seas) occurs because the density of surface water is too low to sink at normal latitudes (that is, around 60° N). The gradual recovery and eventual restoration (*c*) of the overturning intensity, which follows the rapid initial fluctuation, is attributable partly to the vertical subsurface water column of relatively high density which is restored in the sinking region of the THC by ~70 years of the experiment. The increase of the water column density is due not only to the horizontal spreading and disappearance of the very fresh surface water but also to the reduced supply of warm water with relatively low density from the south into the sinking region of the THC. The gradual reintensification of the THC is also attributable to the reduction of subsurface water density in low latitudes which is due to the weakened upwelling of dense water associated with the large initial weakening of the THC. The increase in the meridional gradient of density due to the density changes of opposite sign in the sinking and rising regions of the THC results in the increase of not only the meridional but also the zonal density gradient[20] in the upper layer of the ocean, intensifying the meridional circulation and causing the gradual recovery in the intensity of the THC.

Manabe and Stouffer, Nature, 1995

Response of the THC to moisture flux trend and stochastic wind forcing

- results from three realizations

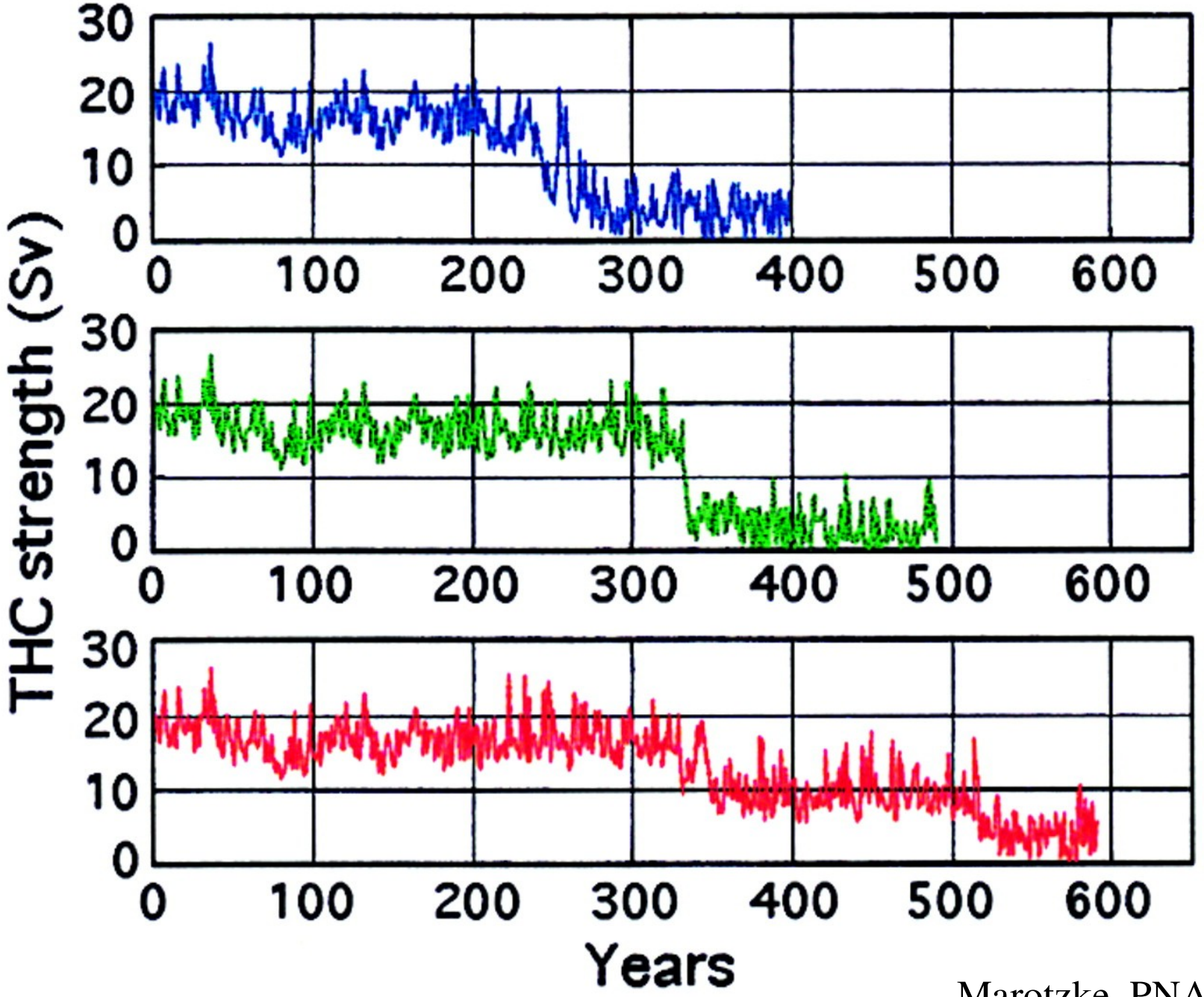

Marotzke, PNAS, 2000

Response of the Stommel model to stochastic forcing

$$\frac{d}{dt}\Delta T = -t_r^{-1}(\Delta T - \theta) - Q(\Delta\rho)\Delta T$$

$$\frac{d}{dt}\Delta S = \frac{F(t)}{H} S_0 - Q(\Delta\rho)\Delta S. \qquad (2.3)$$

$$Q_1 = t_d^{-1}, \quad Q_2 = t_d^{-1} + V^{-1}q|\Delta\rho|,$$
$$Q_3 = t_d^{-1} + V^{-1}q(\Delta\rho)^2. \quad (2.4)$$

Cessi, JPO, 1994

Salinity performs a random walk in a double-welled potential

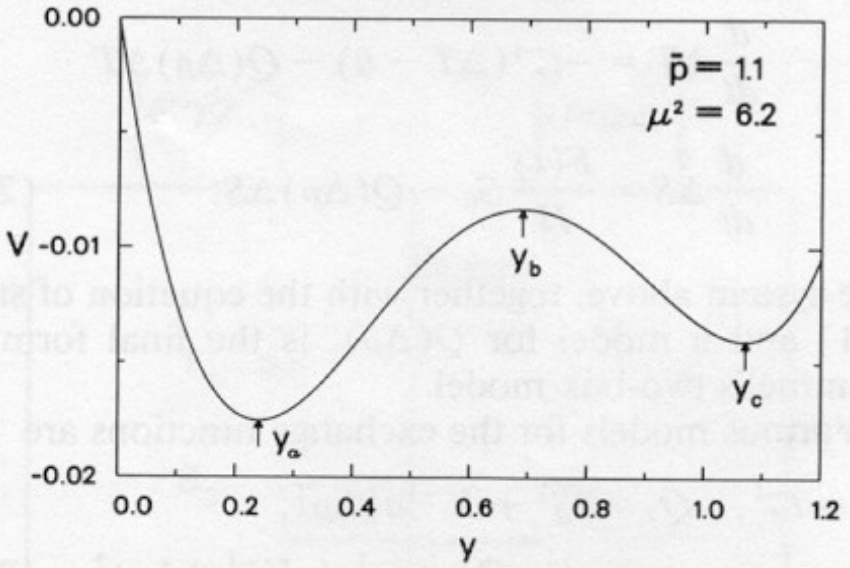

FIG. 2. The potential V defined in (2.9) as a function of the salinity gradient y. The steady states of (2.8b) with $p' = 0$ are extrema of V. The global minimum, located at $y_a \approx 0.24$ is linearly stable, as is the local minimum at $y_c \approx 1.07$. However, the latter is a metastable equilibrium, and a generic finite amplitude perturbation will move the system to y_a. The maximum, located at $y_b \approx 0.69$, is linearly unstable.

$$V(y) \equiv \mu^2\left(\frac{y^4}{4} - \frac{2}{3}y^3 + \frac{y^2}{2}\right) + \frac{y^2}{2} - \bar{p}y, \quad (2.9)$$

Cessi, JPO,

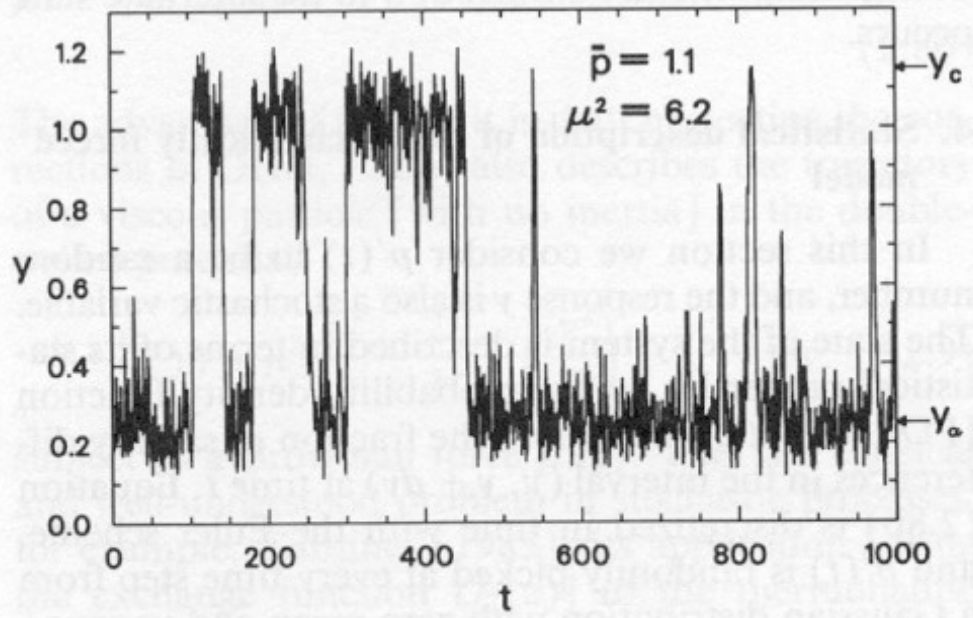

FIG. 5. A typical time series of y solution of (2.8b). At every time step, of size $dt = 3.33 \times 10^{-3}$, the stochastic forcing is randomly picked from a Gaussian distribution with zero mean and standard deviation $\sigma = 3.3$. The values of $\bar{p}$ and μ^2 are as in Fig. 2. The salinity difference y spends most of the time in the neighborhood of the stable states y_a and y_c.

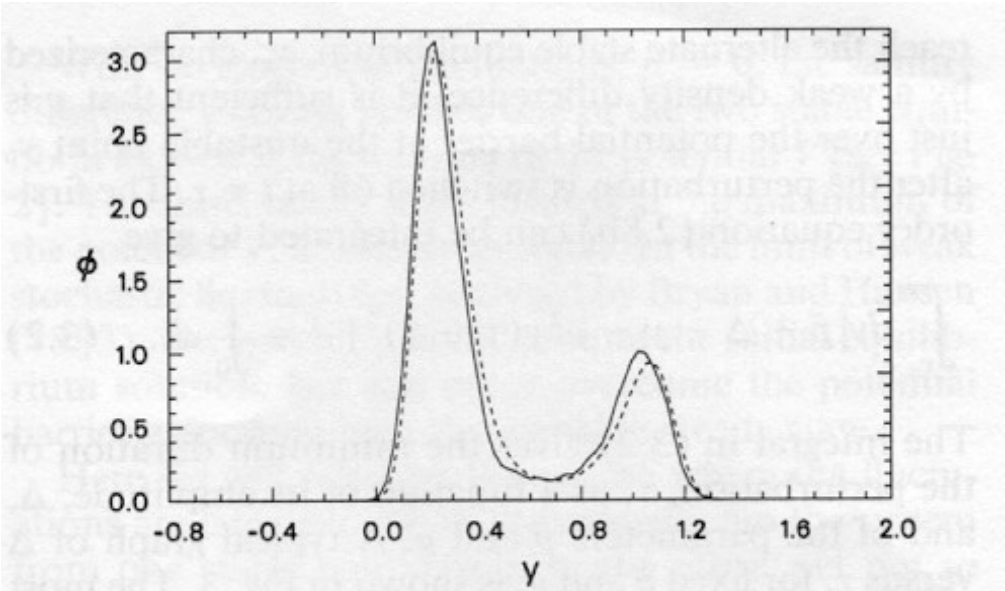

FIG. 6. The stationary PDF (4.6) (dashed line) is in good agreement with the PDF resulting from numerical simulation (solid line). To estimate the "true" PDF we have binned the values of salinity difference shown in Fig. 5.

Cessi, JPO, 1994

Note differences of responses of linear oscillator and system with multiple steady states:

increase of amplitude of stochastic forcing ....

Linear oscillator:

.... increases amplitude of response, and leaves intrinsic frequency unchanged

Multiple steady states:

... leaves amplitude roughly unchanged, but reduces the intrinsic frequency.

Examples of Rapid Climate Shifts

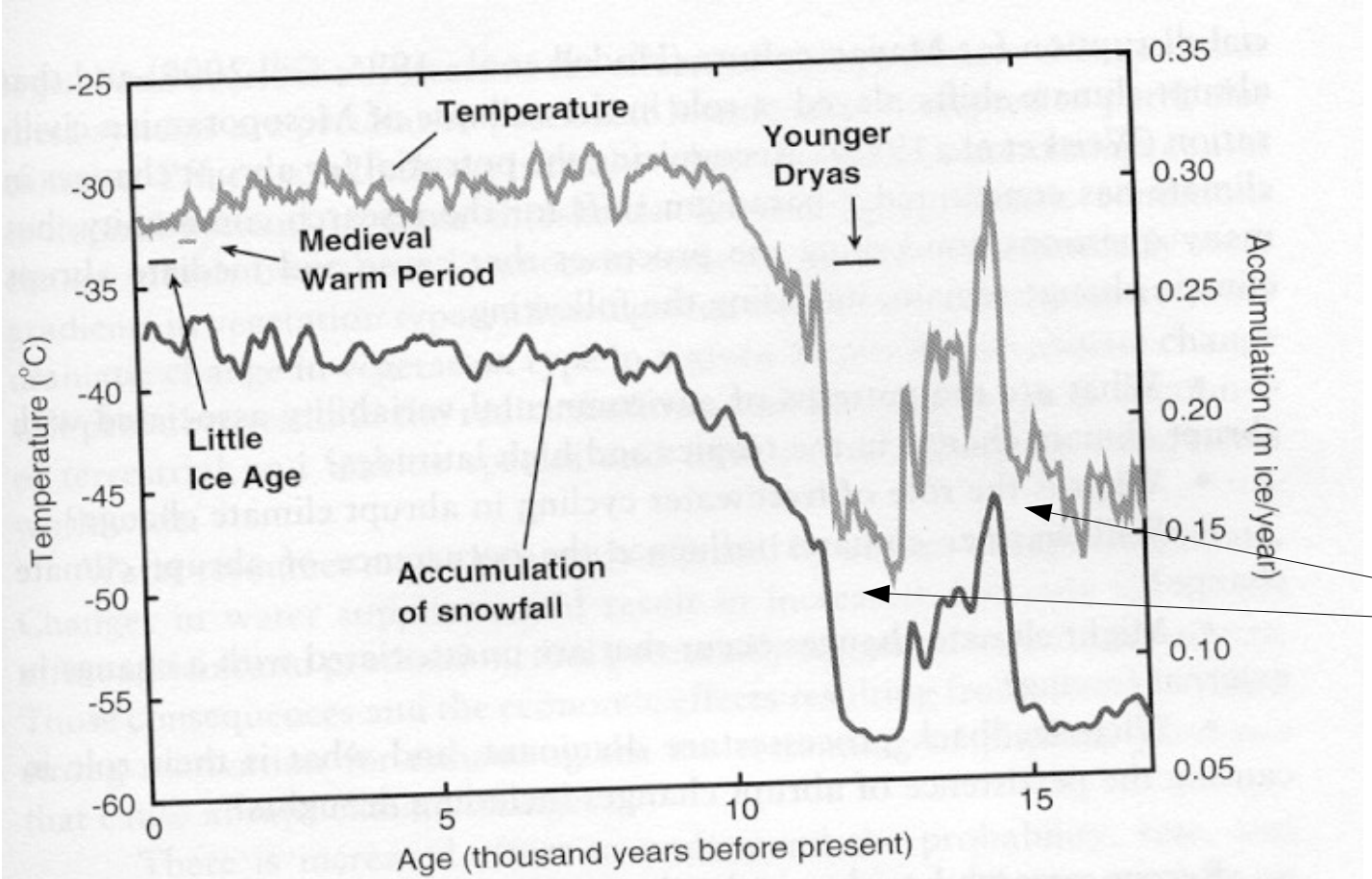

FIGURE 1.2 Climate changes in central Greenland over the last 17,000 years. Reconstructions of temperature and snow accumulation rate (Cuffey and Clow, 1997; Alley, 2000) show a large and rapid shift out of the ice age about 15,000 years ago, an irregular cooling into the Younger Dryas event, and the abrupt shift toward modern values. The 100-year averages shown somewhat obscure the rapidity of the shifts. Most of the warming from the Younger Dryas required about 10 years, with 3 years for the accumulation-rate increase (Figure 2.2). A short-lived cooling of about 6°C occurred about 8,200 years ago (labeled 8ka event), and is shown with higher time resolution in Figure 2.3. Climate changes synchronous with those in Greenland affected much of the world, as shown in Figures 2.1 and 2.3.

Note rapid changes

Alley et al., Abrupt Climate Change, NAP, 2002

Changes are wide spread, very rapid, and are found in many variables

Cariaco basin

Greenland Ice core

Methane

Sea salt: winds

Calcium: continental dust

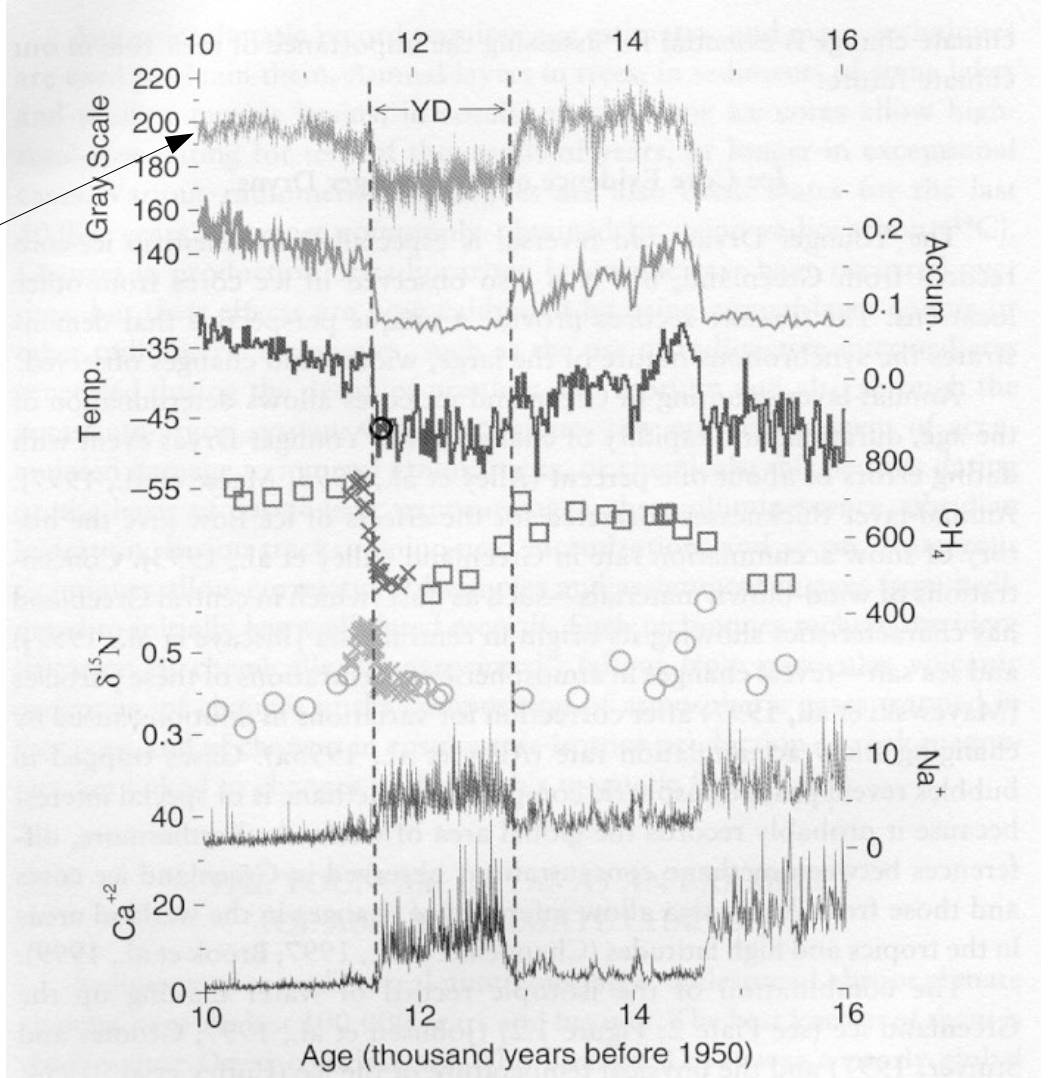

FIGURE 2.1 The Younger Dryas (YD) climate event, as recorded in an ice core from central Greenland and a sediment core from offshore Venezuela. The uppermost curve is the gray-scale (light or dark appearance) of the Cariaco Basin core, and probably records changes in windiness and rainfall (Hughen et al., 1998). The other curves are from the GISP2, Greenland ice core. The rate of snow accumulation and the temperature in central Greenland were calculated by Cuffey and Clow (1997), using the layer-thickness data from Alley et al. (1993) and the ice-isotopic ratios from Grootes and Stuiver (1997), respectively. The independent Severinghaus et al. (1998) temperature estimate is shown by the circle near the end of the Younger Dryas. Methane data are from Brook et al. (1996) (squares) and Severinghaus et al. (1998) (x), and probably record changes in global wetland area. Changes in the $\delta^{15}N$ values as measured by Severinghaus et al. (1998) record the temperature difference between the surface of the Greenland ice sheet and the depth at which bubbles were trapped; abrupt warmings caused the short-lived spikes in this value

Alley et al., Abrupt Climate Change, NAP, 2002

Changes might occur in as little as a few years ...

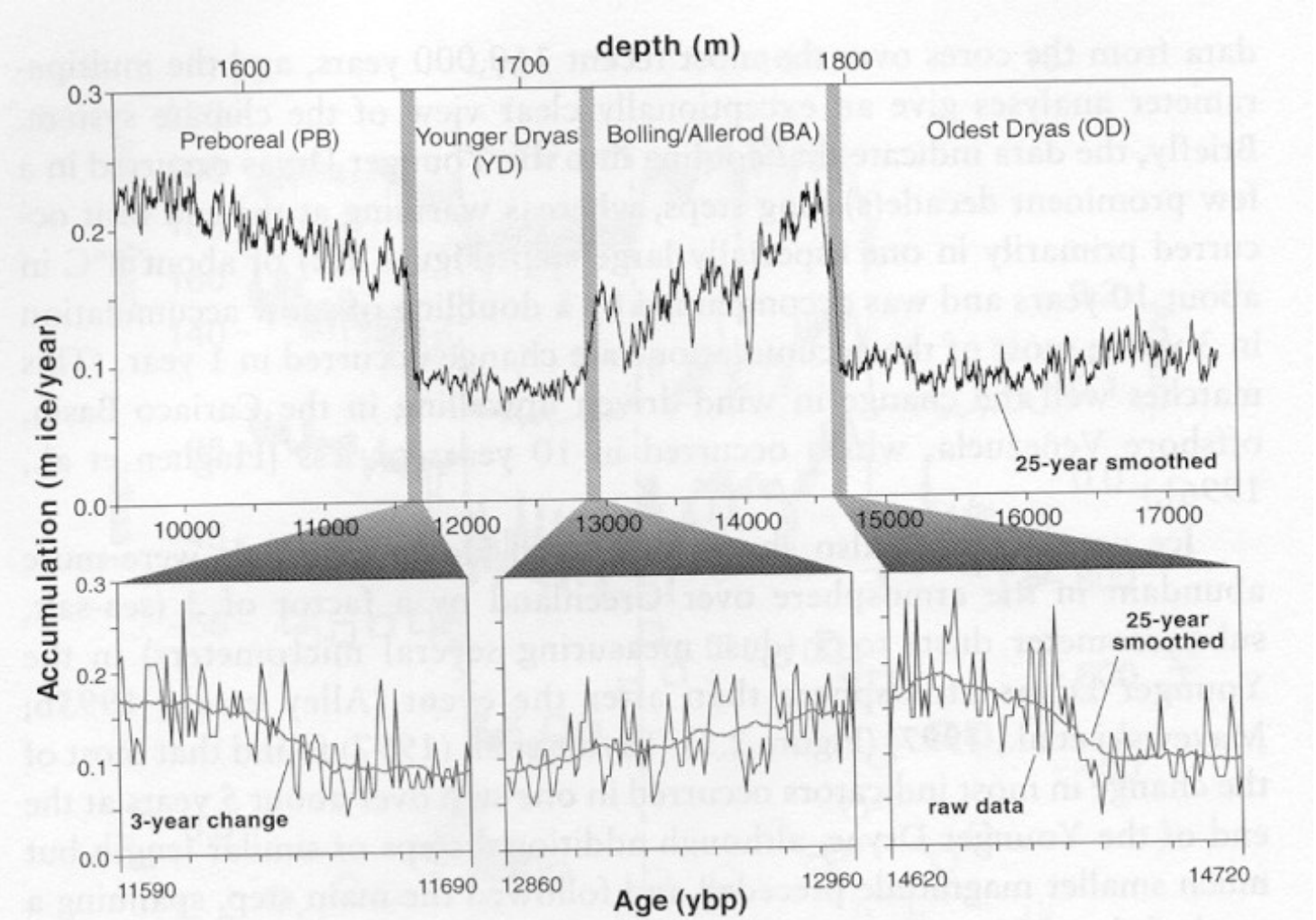

FIGURE 2.2 The accumulation rate of ice in Greenland was low during the Younger Dryas, and both the start and end of the period show as abrupt changes. Modified from Alley et al. (1993).

Alley et al., Abrupt Climate Change, NAP, 2002

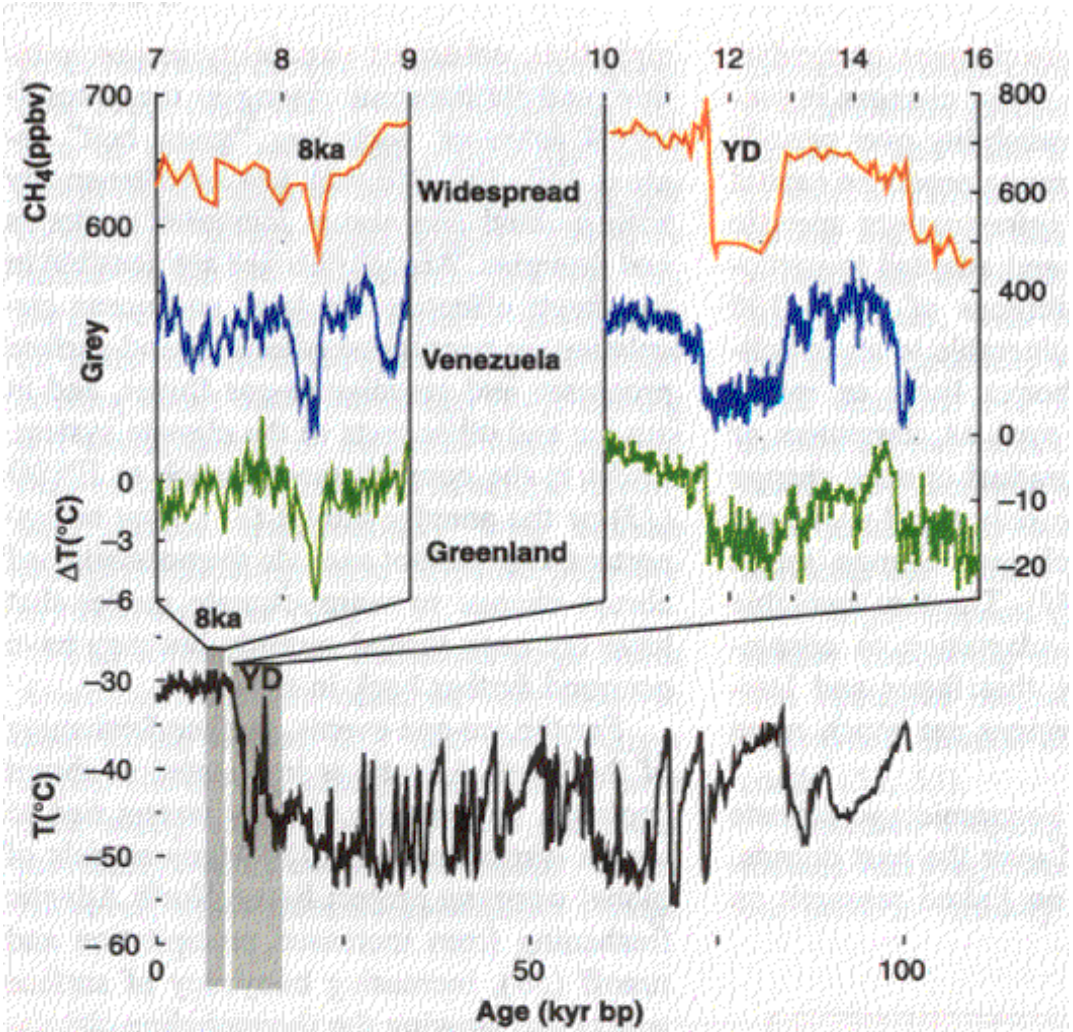

Fig. 3. Paleoclimatic data showing abrupt climate changes, after (*45*) and other sources. The lower panel is the history of temperature in central Greenland over the last 110,000 years (*72*). Details of temperature for the Younger Dryas (YD) event and for the cold event about 8200 years ago (8ka) are shown as deviations from the temperature averaged over the intervals from 7000 to 8000 and 8400 to 9000 years ago. Methane concentrations (*23*) reflect production in global wetlands, including important tropical sources. Gray-scale of a sediment core from the Cariaco Basin, offshore Venezuela (*73*), is plotted here so that a downward shift corresponds to the effects of stronger winds over the basin or decreased rainfall on adjacent land. Note differences in scales in the detailed figures; the scale for the Cariaco Basin record is not shown, but has twice the range for the YD as for the 8ka.

Alley et al., Science, 2003

Rapid climate cooling 8200 years ago, likely caused by outburst flooding around melting ice sheet in Hudson Bay.

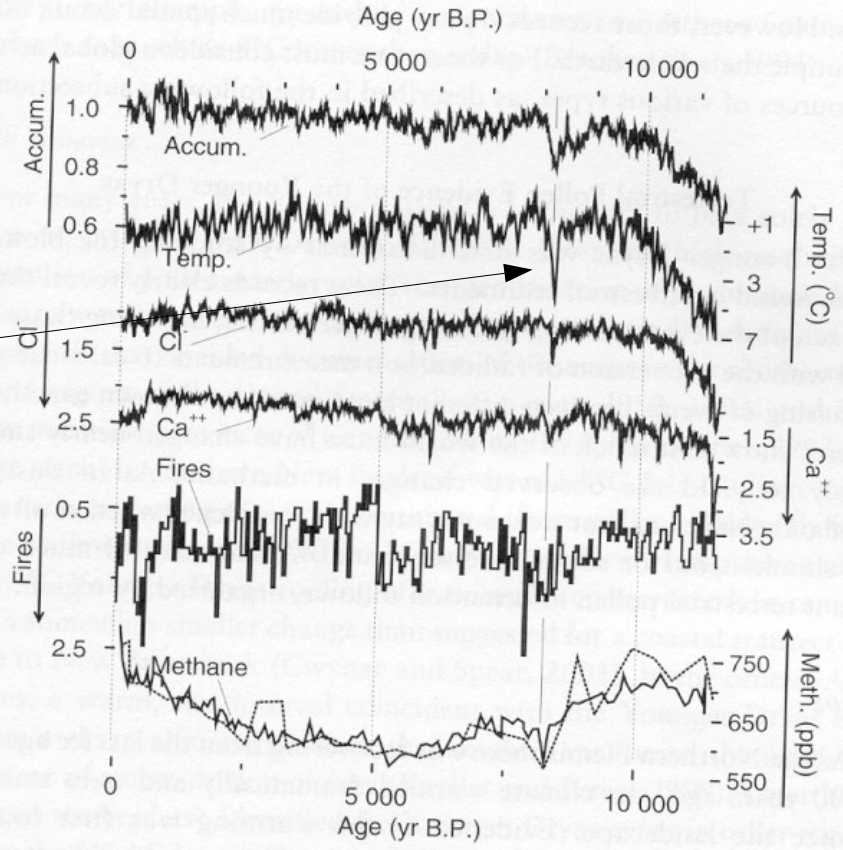

FIGURE 2.3 Climate data from the GISP2 core, central Greenland, showing changes about 8,200 years ago probably caused by outburst flooding from around the melting ice sheet in Hudson Bay (Barber et al., 1999) and affecting widespread regions of the globe. The event punctuated generally warm conditions not too different from recently, so warmth is not a guarantee of climate stability. Accumulation and temperature reflect conditions in Greenland, chloride is wind-blown sea-salt from beyond Greenland, and calcium is continental dust probably from Asia (Biscaye et al., 1997). Forest-fire smoke likely is from North America, and methane probably records global wetland area. Data are shown as approximately 50-year running means. Accumulation from Alley et al. (1993) and Spinelli (1996), chloride and calcium from O'Brien et al. (1995), and fire data shown as a 50-year histogram of frequency of fallout from fires (Taylor et al., 1996), expressed as ratios to their average values during the approximately 2,000 years just prior to the Little Ice Age. Temperature is calculated as a deviation from the average over the same 2,000 years, from oxygen-isotopic data of ice (Stuiver et al., 1995), assuming a calibration of 0.33 per mil per degree C (Cuffey et al., 1995). Methane concentrations from the GISP2 core (heavier line; Brook et al., 1996) and the GRIP core (Blunier et al., 1995) are shown in parts per billion by volume (ppb). Note that some scales increase upward and others downward, as indicated, so that all curves vary together at the major events. Modified from Alley et al. (1997).

Alley et al., Abrupt Climate Change, NAP, 2002

Global extent of rapid change

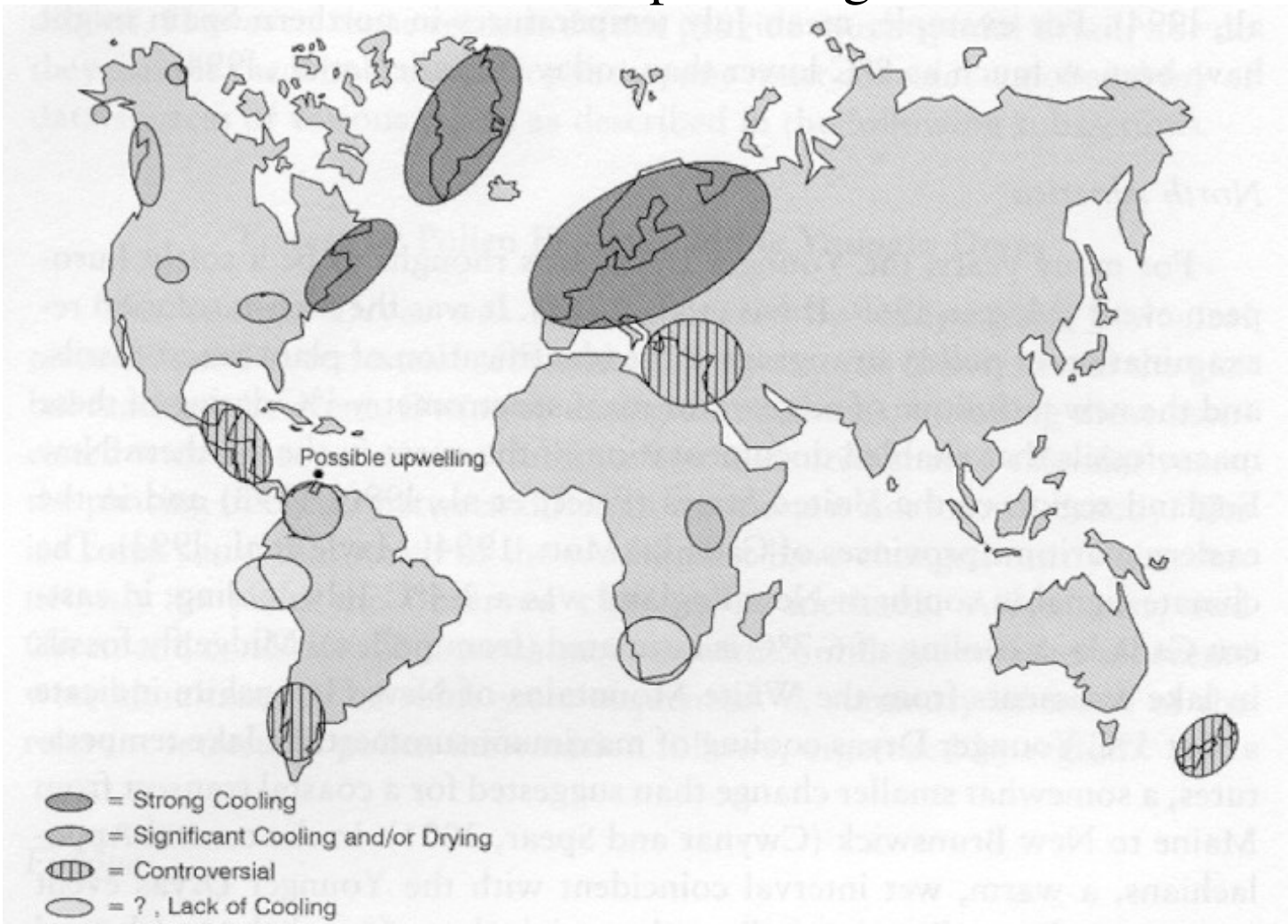

FIGURE 2.4 Global extent of terrestrial (pollen) and ice core (isotopic) evidence where the Younger Dryas cooling (11,500 – 13,000 BP) has been found. While northern hemispheric evidence is consistently strong for cooling, southern hemispheric sites contain controversial evidence and in some cases lack of evidence for a cooling during the YD interval. Possible upwelling in the Cariaco Basin during this time is also indicated, attributed to trade wind increase. Strong cooling ranges from 13-4° C; controversial means some sites show cooling and some do not (after Peteet, 1995).

Alley et al., Abrupt Climate Change, NAP, 2002

Long history of rapid temperature fluctuations: Dansgaard/Oeschger oscillations

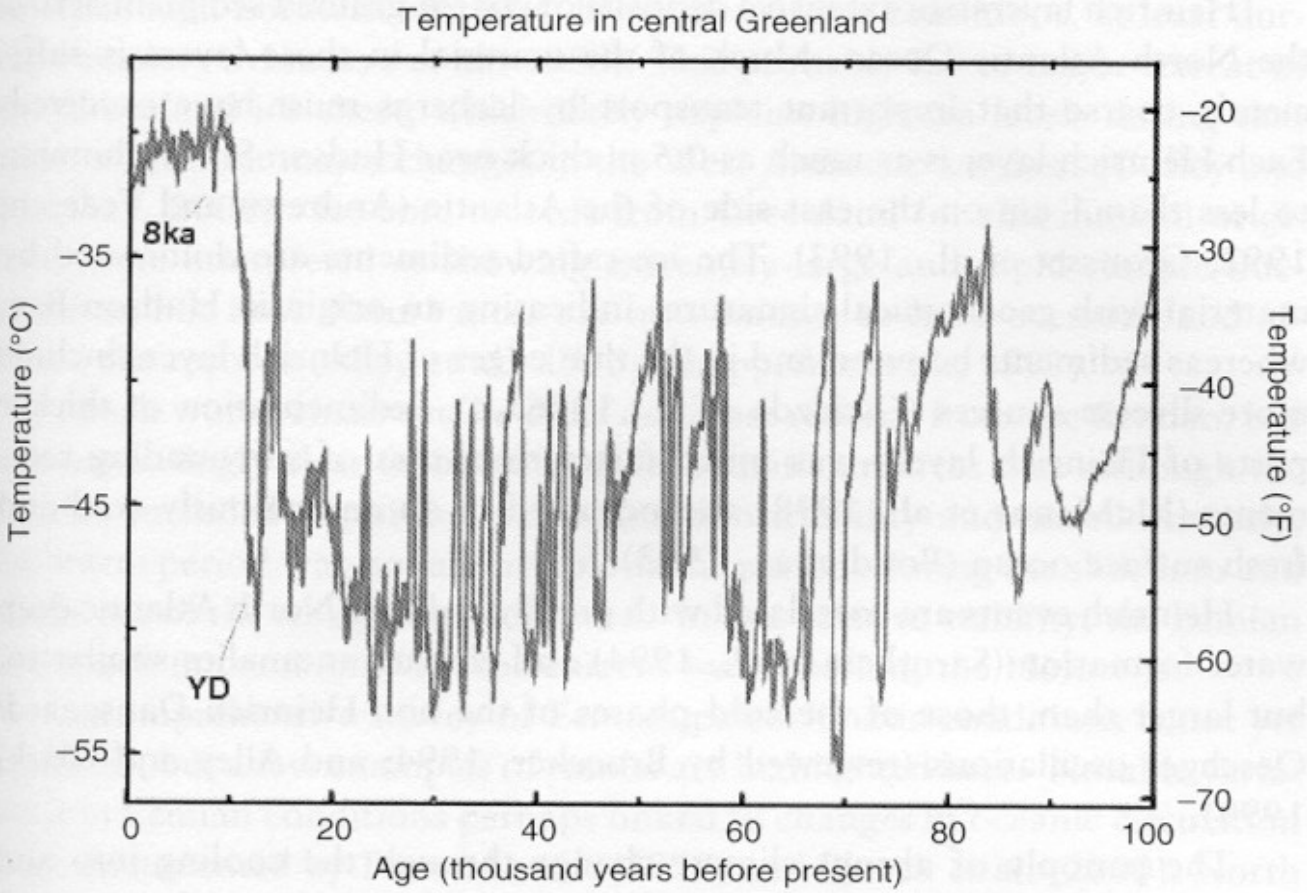

FIGURE 2.5 History of temperature in central Greenland over the last 100,000 years, as calculated by Cuffey and Clow (1997) from the data of Grootes and Stuiver (1997). The large Younger Dryas temperature oscillation (labeled YD), and the smaller temperature change of the event about 8,200 years ago (labeled 8ka) are just the most recent in a long sequence of such abrupt temperature jumps. Changes in materials from beyond Greenland trapped in the ice cores, including dust and methane, demonstrate that just as for the YD and 8ka events, the earlier events affected large areas of the earth nearly simultaneously.

Alley et al., Abrupt Climate Change, NAP, 2002

Ice ages occur on both hemisphere, often at similar times

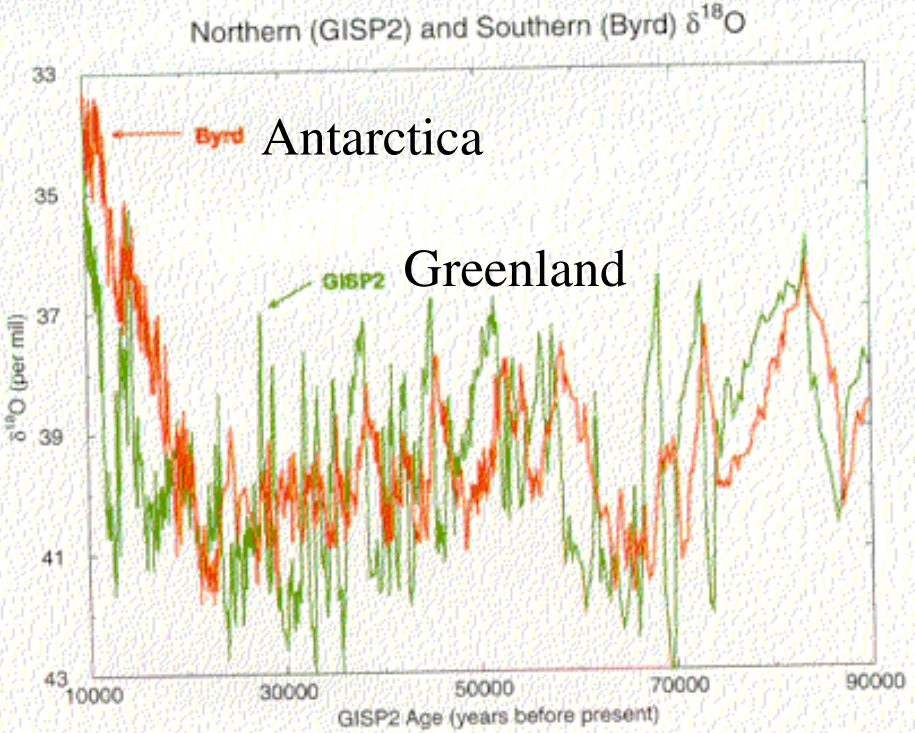

PLATE 2 Temperature changes are reflected in changes in the oxygen-isotopic ($\delta^{18}O$) ratios, with low $\delta^{18}O$ indicating high temperature. Records of $\delta^{18}O$ from ice cores in central Greenland (GISP2) and West Antarctica (Byrd Station) are shown, synchronized to the GISP2 time scale by Blunier and Brook (2001). These records show that both hemispheres experienced an ice age at similar time, that millennial oscillations superimposed on the ice-age cycle were especially large during the slide into and climb out of the ice age, that millennial oscillations were of larger amplitude in the north than in the south, and that at many times (e.g., around 70,000 years ago) antiphase behavior is exhibited between north and south in these millennial oscillations. Note that in this figure, time increases toward the left.

Alley et al., Abrupt Climate Change, NAP, 2002

Rapid climate variations in more recent past:

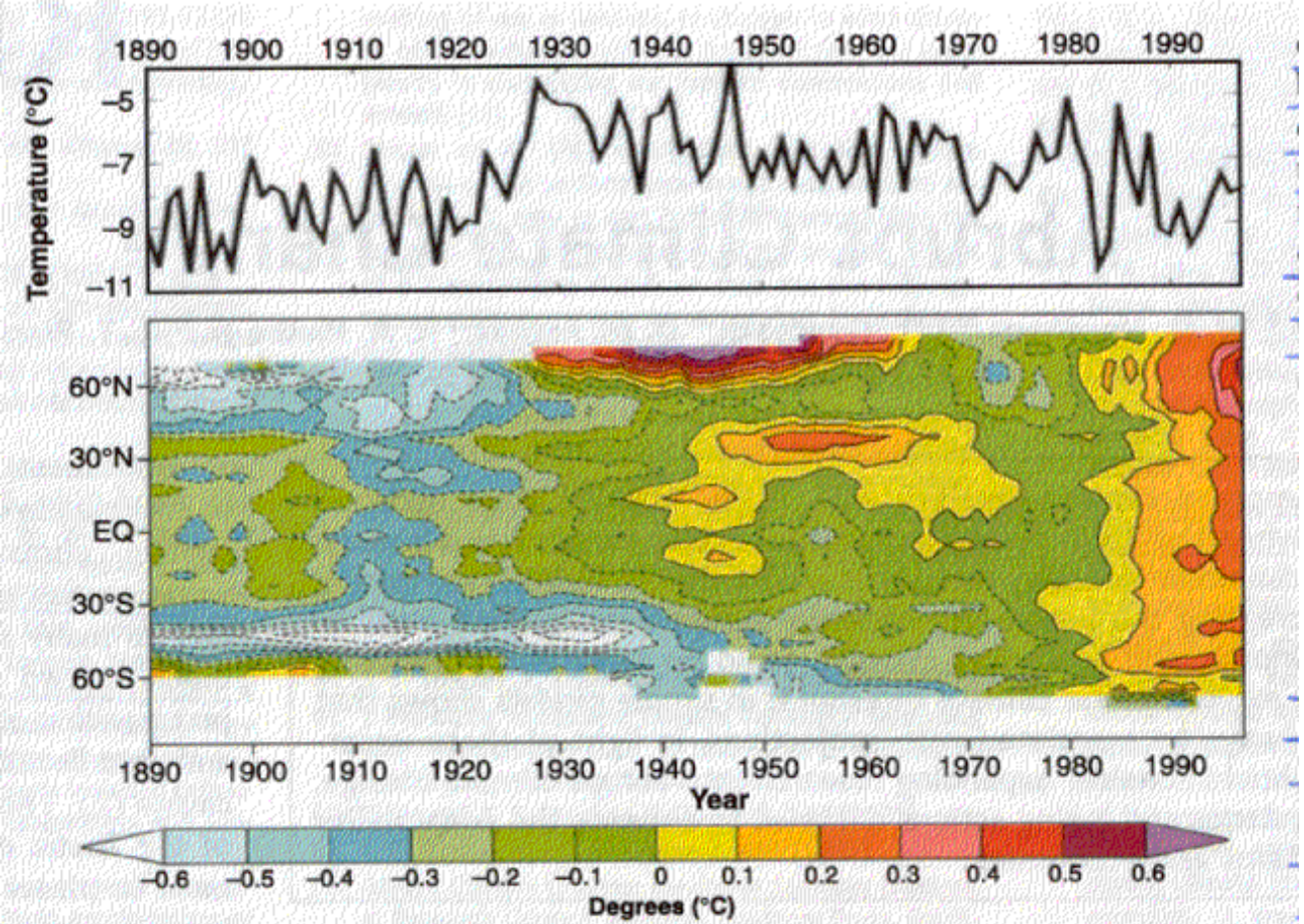

Fig. 1. Observed, zonally averaged, land-surface air-temperature anomalies (°C) as a function of latitude and time (*7*), together with the temperature record for the same interval from Upernavik, Greenland (72°47′N, 56°10′W, on the northwest coast of Greenland) (*8*). Global instrumental coverage is just sufficient to capture the rapid, concentrated warming at high northern latitudes in the 1920s, which is shown more dramatically at sites such as Upernavik.

Alley et al., Science, 2003

Droughts in North America

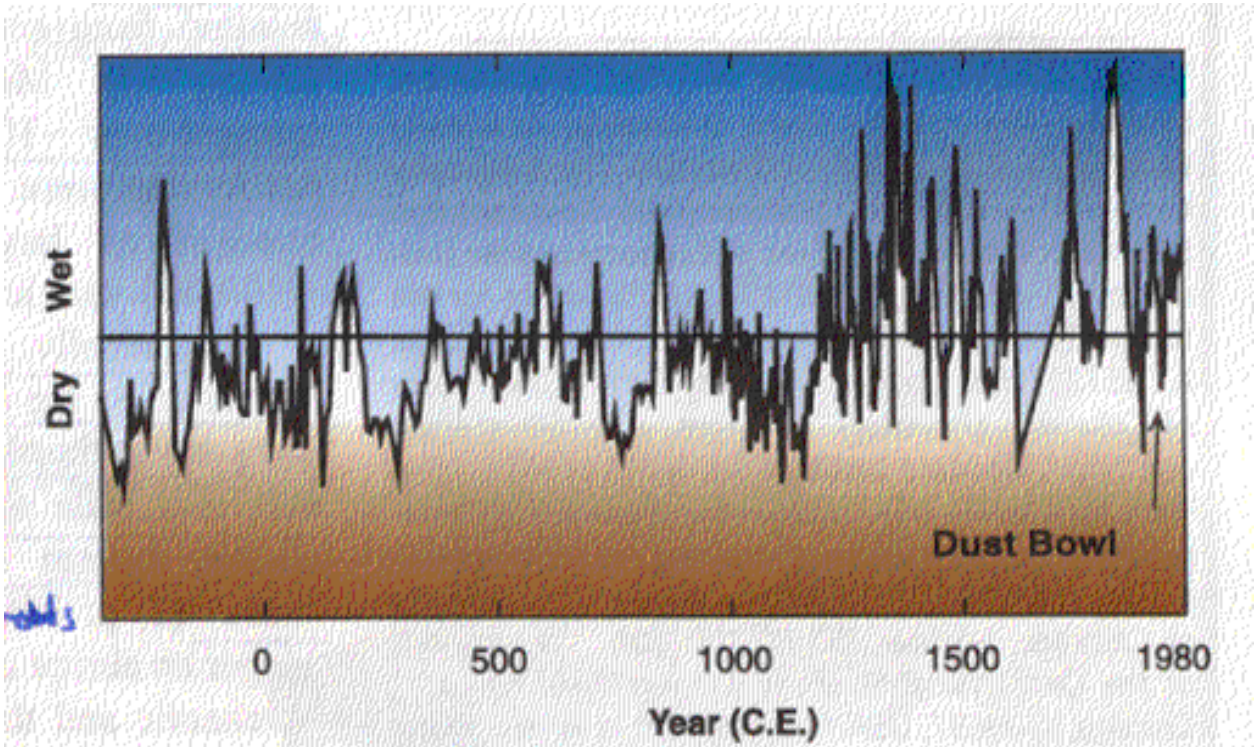

Fig. 2. Salinity of Moon Lake, North Dakota, USA (46°51′27″N, 98°09′30″W) derived from diatom records (*71*). The Dust Bowl drought of the 1930s is shown clearly by increased lake salinity, but larger and longer droughts, often with abrupt onsets, occurred frequently before ~1200.

Alley et al., Science, 2003

Possible causes, triggers:

orbital forcing

outburst floods

greenhouse gases

continental drift

Amplifiers:

ice-albedo feedback

vegetation-hydrological feedback: evapo-transpiration

ocean convection

Persistence:

Thermohaline circulation

root-runoff feedback

Globalization

Alley et al., Science, 2003

Box 3.1
Thresholds and Hysteresis

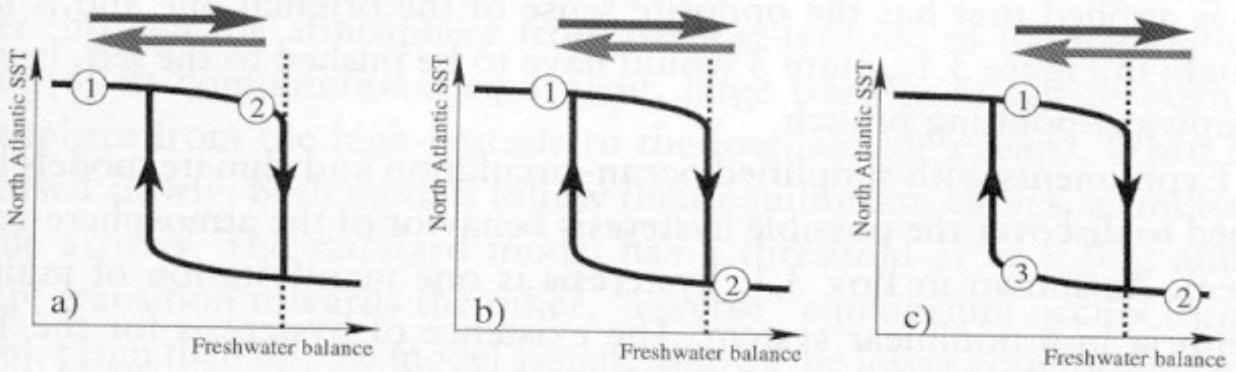

FIGURE 3.1

Many simple physical systems exhibit abrupt change, as demonstrated in the simple diagram presented in Box 1.1. The more complex figure (Figure 3.1) provides a schematic view of hysteresis in the thermohaline circulation. The upper branch denotes climate states in which the THC is strong and North Atlantic temperatures are relatively high (similar to present conditions). The lower branch represents a much-reduced or collapsed THC, in which the Atlantic meridional heat flux by the ocean is small. A given perturbation (indicated by the horizontal arrows) in the freshwater balance of the North Atlantic (precipitation plus runoff minus evaporation) first causes transitions from an initial state 1 to state 2. The reverse perturbation then causes a transition back to state 1, or to state 3. Three structurally different responses are possible for the same pair of perturbations, depending on whether threshold values (dashed line) are crossed. This, in turn, depends on where state 1 is, relative to the threshold: a) small, reversible response; b) large, reversible response; c) large, irreversible response (Stocker and Marchal, 2000).

Alley et al., Abrupt Climate Change, NAP, 2002

Response of THC to change in radiative forcing

System close to threshold: low predictability

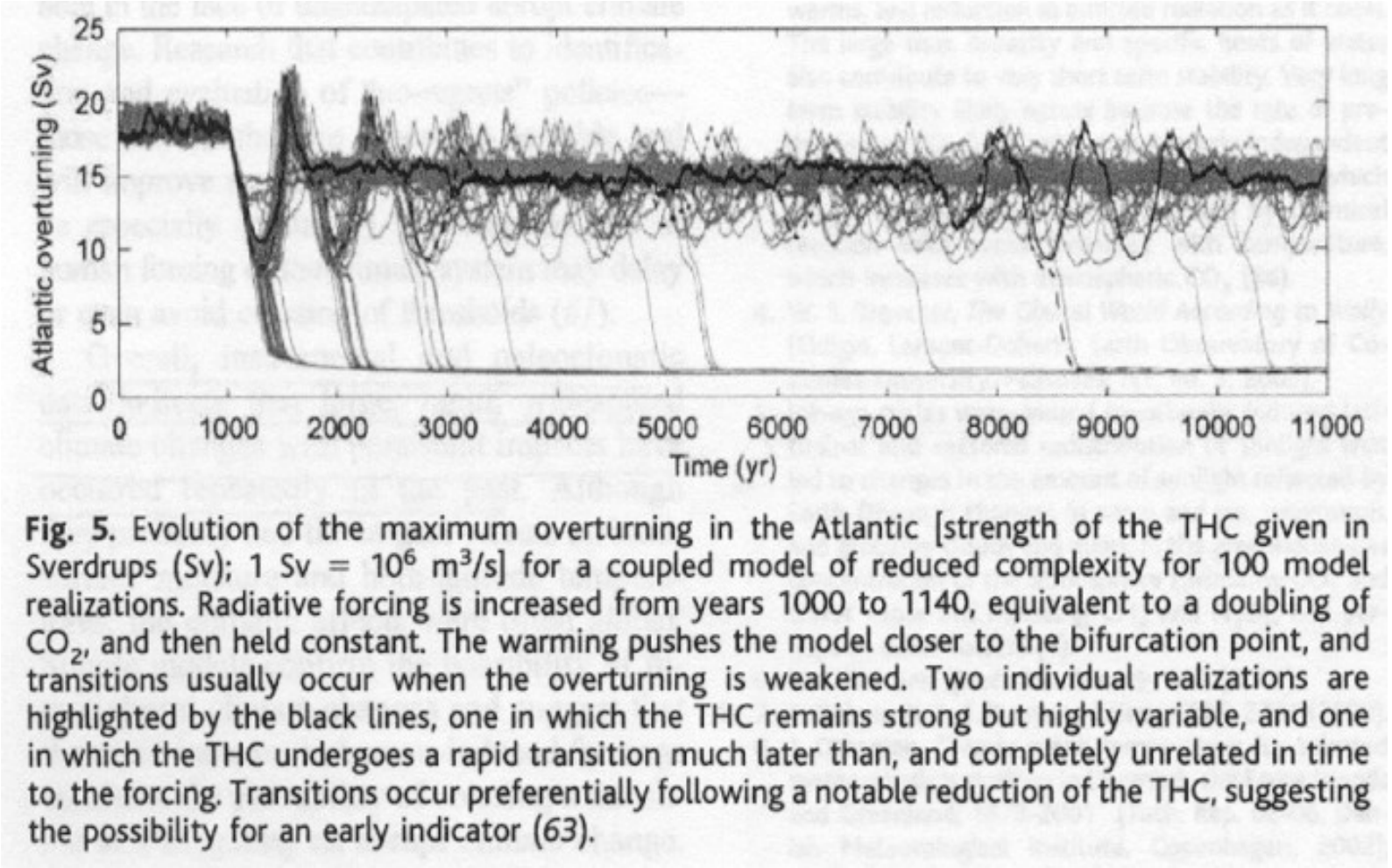

Fig. 5. Evolution of the maximum overturning in the Atlantic [strength of the THC given in Sverdrups (Sv); 1 Sv = 10^6 m^3/s] for a coupled model of reduced complexity for 100 model realizations. Radiative forcing is increased from years 1000 to 1140, equivalent to a doubling of CO_2, and then held constant. The warming pushes the model closer to the bifurcation point, and transitions usually occur when the overturning is weakened. Two individual realizations are highlighted by the black lines, one in which the THC remains strong but highly variable, and one in which the THC undergoes a rapid transition much later than, and completely unrelated in time to, the forcing. Transitions occur preferentially following a notable reduction of the THC, suggesting the possibility for an early indicator (*63*).

Alley et al., Science, 2003

Response of THC to changes of CO2

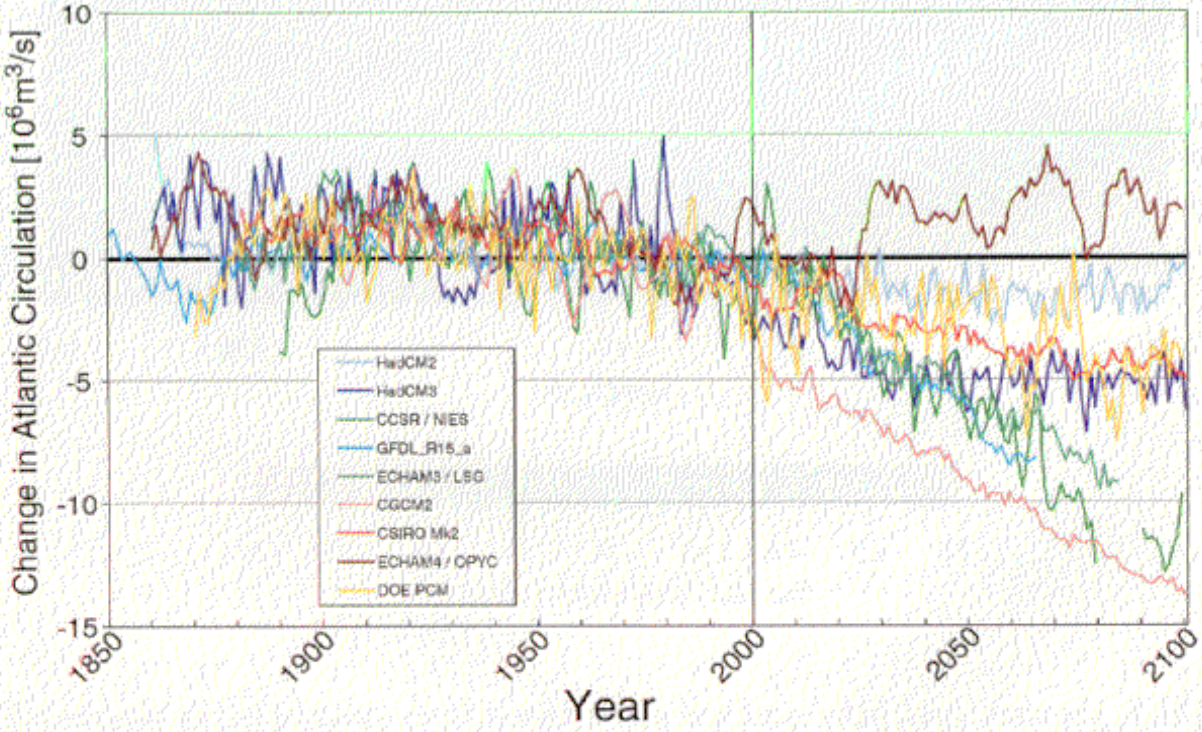

PLATE 7 Changes in Atlantic circulation in different models forced by prescribed increases in atmospheric CO_2. Most models show a reduction of the THC in response to increasing greenhouse gas forcing (Intergovernmental Panel on Climate Change, 2001b).

Warmer atmosphere leads to a wetter atmosphere and increased moisture transport from low to high latitudes. Increased precipitation in the North Atlantic freshens the waters and reduce surface density, interrupting deep convection and slowing the THC.

Alley et al., Abrupt Climate Change, NAP, 2002

Response of THC to a freshwater pulse

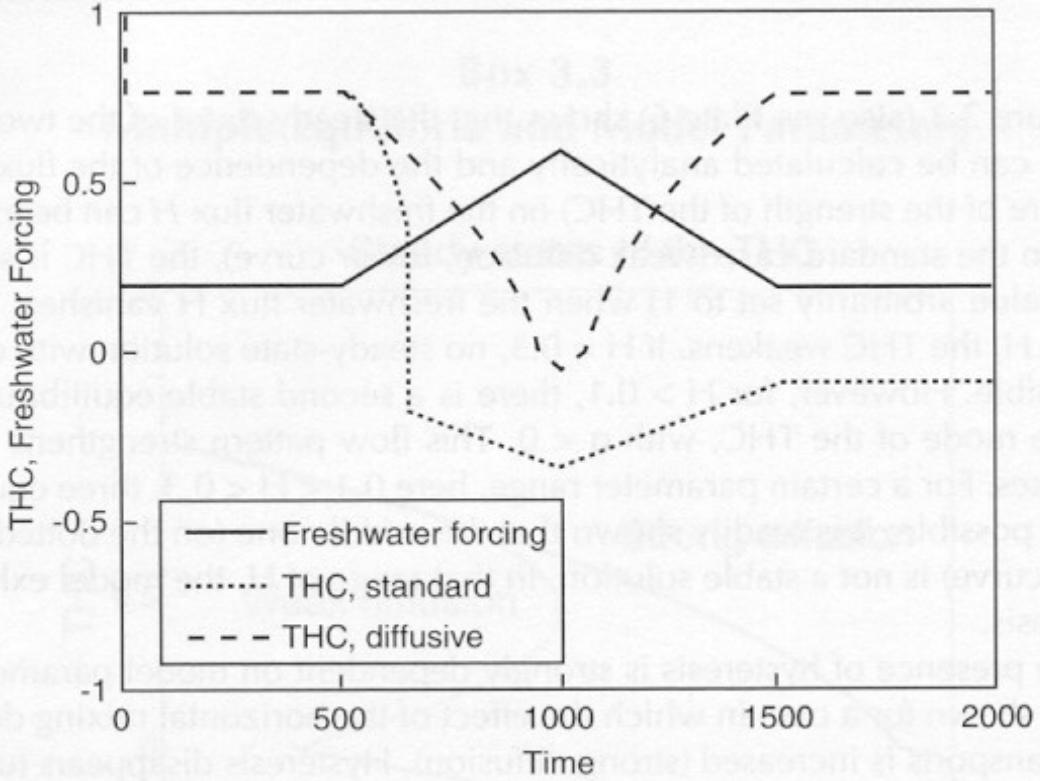

FIGURE 3.4 Response to the thermohaline circulation (THC) to a slow increase and subsequent slow decrease in freshwater forcing for the two cases in Figure 3.3.

Alley et al., Abrupt Climate Change, NAP, 2002